

**FAST RADIO BURSTS: DETECTION WITH PYTHON LANGUAGE
RADIO BURST EMISSION AUTOMATIC ROGER (POLAR BEAR)**

AFFAN ADLY BIN NAZRI

**DEPARTMENT OF PHYSICS
FACULTY OF SCIENCE
UNIVERSITY OF MALAYA
KUALA LUMPUR**

2021

**FAST RADIO BURSTS: DETECTION WITH PYTHON
LANGUAGE RADIO BURST EMISSION AUTOMATIC
ROGER (POLAR BEAR)**

AFFAN ADLY BIN NAZRI

**THESIS SUBMITTED IN FULFILMENT OF THE
REQUIREMENTS FOR THE DEGREE OF BACHELOR**

**DEPARTMENT OF PHYSICS
FACULTY OF SCIENCE
UNIVERSITY OF MALAYA
KUALA LUMPUR**

2021

UNIVERSITI MALAYA

ORIGINAL LITERARY WORK DECLARATION

Name of Candidate: Affan Adly bin Nazri (I.C./Passport No.: 991023105711)

Registration/Matric No.: 17169864

Name of Degree: Bachelor of Science in Physics

Title of Project Paper/Research Report/Dissertation/Thesis ("this Work"):

Fast Radio Bursts: Detection with Python Language Radio Burst Emission Automatic

Roger (PoLaR BEAR)

Field of Study: Astrophysics & Radio Astronomy

I do solemnly and sincerely declare that:

- (1) I am the sole author/writer of this Work;
- (2) This work is original;
- (3) Any use of any work in which copyright exists was done by way of fair dealing and for permitted purposes and any excerpt or extract from, or reference to or reproduction of any copyright work has been disclosed expressly and sufficiently and the title of the Work and its authorship have been acknowledged in this Work;
- (4) I do not have any actual knowledge nor do I ought reasonably to know that the making of this work constitutes an infringement of any copyright work;
- (5) I hereby assign all and every rights in the copyright to this Work to the University of Malaya ("UM"), who henceforth shall be owner of the copyright in this Work and that any reproduction or use in any form or by any means whatsoever is prohibited without the written consent of UM having been first had and obtained;
- (6) I am fully aware that if in the course of making this Work I have infringed any copyright whether intentionally or otherwise, I may be subject to legal action or any other action as may be determined by UM.

Candidate's Signature

Date:

Subscribed and solemnly declared before,

Witness's Signature

Date:

Name:

Designation:

**FAST RADIO BURSTS: DETECTION WITH PYTHON LANGUAGE RADIO
BURST EMISSION AUTOMATIC ROGER (POLAR BEAR)**

ABSTRACT

Fast radio bursts (FRB) are bright, broadband radio emissions with durations of milliseconds or less. These mysterious astrophysical phenomena are characterized by their frequency-dependent delay in the signal, also known as dispersion measure or DM. Almost all FRBs detected have DMs more than the contribution from the Milky Way, suggesting that they are extragalactic. The exact source of FRBs is uncertain, but most evidence seem to point towards magnetars, which are neutron stars with strong magnetic fields. Finding a larger sample of FRBs would be paramount in confirming and understanding the exact progenitor and burst mechanism for FRBs. Here, a Python program to detect FRBs in radio telescope data is developed based on BEAR. The program performs various functions, most importantly RFI mitigation, dedispersion, and matched filtering based on the likelihood statistic ratio test. The program then outputs FRB candidates which are detected in the data. The program manages to detect all FRBs in the real FRB data and generated FRB data with deviations comparable to BEAR. The program is expected to provide a simpler understanding in the FRB detection methodology.

Key words: astrophysics – transients: fast radio bursts – methods: data analysis

ABSTRAK

Gelombang radio sejenak atau *Fast radio bursts* (FRB) ialah pancaran radio jalur lebar yang terang dengan jangka masa milisaat atau kurang. Fenomena astrofizik misteri ini diclasifikasikan oleh kelewatan isyarat yang mana ia bergantung pada frekuensi, juga dikenali sebagai ukuran penyebaran atau *dispersion measure* (DM). Hampir kesemua FRB yang telah dikesan mempunyai DM yang mana penyebarannya melebihi daripada apa yang disumbangkan oleh Bima Sakti. Ini menjadi bukti bahawa FRB berasal dari luar Bima Sakti. Punca sebenar FRB masih tidak dapat diketahui, tetapi kebanyakan petanda menunjukkan FRB mungkin berasal dari *magnetar* iaitu bintang neutron yang mempunyai medan magnet yang sangat kuat. Bagi mengesahkan dan memahami asal usul dan mekanisme emisi FRB, lebih banyak sampel FRB diperlukan. Dalam kajian ini, sebuah program untuk mengesan FRB daripada data teleskop radio telah dihasilkan menggunakan *Python* berdasarkan program BEAR. Antara fungsi penting yang dijalankan dalam program ini ialah pebatan RFI atau *RFI mitigation*, penyah-sebaran atau *dedispersion*, dan penurasan padan atau *matched filtering* berdasarkan ujian nisbah statistik kemungkinan. Program tersebut menghasilkan calon-calon FRB yang dikesan terdapat dalam data. Program tersebut berjaya mengesan semua FRB daripada data FRB sebenar dan data FRB yang terjana dengan sisihan setanding BEAR. Program ini diharap dapat memberikan pemahaman yang lebih mudah dalam metodologi pengesanan FRB.

ACKNOWLEDGEMENTS

In the name of Allah, the Most Gracious and the Most Merciful.

All praises to Allah for the strengths and His blessings in completing this thesis. I would like to first express my very great appreciation to my supervisor, Assoc. Prof. Dr. Zamri Zainal Abidin for his supervision, guidance, and positive reviews in this project. I would also like to thank Mr. Hassan Zakie for his assistance and advice for this project, especially in the technicalities involved. I wish to extend my thanks to all the other members of the Radio Cosmology Lab as well, for keeping the tasks exciting and fun, even in remote and online environments due to the pandemic.

Special thanks to Prof. Lee Ke Jia for his guidance and practical suggestions on the project as well as keeping my progress on schedule. I'd also like to acknowledge Mr. Zhang Chun Feng for his invaluable insight in understanding the mathematical aspects and the original BEAR program itself. In addition, I appreciate all the contributions from the other members of the Pulsar Group of Peking University, as well as researchers and technicians involved in the FRB data collection, especially from the Parkes Telescope.

I would like to express my gratitude to my parents who have instilled me with the love for science at an early age and have supported me ever since, for me to pursue a career in the field. Last but not least, thank you to my close friends and classmates who have given me encouragements and company throughout the project.

TABLE OF CONTENTS

Abstract	iii
Abstrak	iv
Acknowledgements	v
Table of Contents	vi
List of Figures	viii
List of Tables.....	ix
List of Symbols and Abbreviations.....	x
CHAPTER 1: INTRODUCTION	1
1.1 History	1
1.2 Properties of FRBs.....	2
1.3 Progenitor and Emission Theories	3
1.4 Astrophysical Applications	4
1.5 Objectives.....	5
CHAPTER 2: LITERATURE REVIEW	6
2.1 Instrumentation.....	6
2.2 Data Analysis	6
2.3 Pipelines.....	7
CHAPTER 3: METHODOLOGY	9
3.1 Flow of the project	9
3.2 Introduction to PoLaR BEAR.....	10

3.3	Initialization	11
3.4	Pre-analysis	11
3.5	Analysis.....	13
3.6	Output	17
3.7	PoLaR BEAR Tests.....	21
3.7.1	Real FRB data.....	21
3.7.2	Generated FRB data	23
 CHAPTER 4: DATA ANALYSIS AND RESULTS		25
4.1	Real FRB data	25
4.2	Generated FRB data.....	26
4.3	Difference in detections for PoLaR BEAR and BEAR.....	26
4.3.1	Detection DM	26
4.3.2	Detection W.....	28
4.3.3	Detection SNR.....	28
 CHAPTER 5: DISCUSSIONS		30
5.1	Performance Quantization	30
5.2	Underestimation of SNR.....	32
5.3	Differences between PoLaR BEAR and BEAR.....	32
5.4	GPU Dedispersion	34
 CHAPTER 6: SUMMARY		36
	References	38

LIST OF FIGURES

Figure 1.1: Lorimer burst.....	1
Figure 1.2: DMs of FRBs, RRATs, Pulsars	3
Figure 1.3: FRB synchrotron maser emission.....	4
Figure 2.1: PRESTO's pulse processing pipeline output	8
Figure 3.1: Flowchart of the development of the project.	9
Figure 3.2: Block diagram for procedures in PoLaR BEAR.....	10
Figure 3.3: Application of zero-DM matched filter	13
Figure 3.4: Dedispersion	14
Figure 3.5: Example PoLaR BEAR main analysis plot	18
Figure 3.6: Example PoLaR BEAR candidates' pulse profile plots.....	19
Figure 3.7: Example PoLaR BEAR candidates' analysis plot	20
Figure 3.8: Example PoLaR BEAR analysis properties and results	21
Figure 4.1: Histograms of DM difference	26
Figure 4.2: Histograms of W difference.....	28
Figure 4.3: Histograms of SNR difference.....	29
Figure 5.1: PoLaR BEAR candidate output for FRB 010724.....	31
Figure 5.2: SNR deviation due to DM and W offset.....	33
Figure 5.3: Speed-up factor for GPU dedispersion	35

LIST OF TABLES

Table 3.1: Properties of real FRB data.....	22
Table 3.2: Properties of fake FRB data	24
Table 4.1: Detection results for real FRB data	25
Table 4.2: Detection results for fake FRB data	27
Table 5.1: Average deviations in the detection parameters for real FRB data	30
Table 5.2: Average deviations in the detection parameters for fake FRB data.....	30
Table 5.3: Example of a subband dedispersion plan	33

LIST OF SYMBOLS AND ABBREVIATIONS

FRB/FRBs	: Fast radio bursts
DM	: Dispersion measure
RM	: Rotation measure
Jy	: Jansky
pc	: Parsec
FAST	: Five-hundred-meter Aperture Spherical Telescope
CHIME	: Canadian Hydrogen Intensity Mapping Experiment
ASKAP	: Australian Square Kilometer Array Pathfinder
RFI	: Radio frequency interference
ZDMF	: Zero-DM matched filter
SNR	: Signal-to-noise ratio
BEAR	: Burst Emission Automatic Roger
PoLaR BEAR	: Python Language Radio Burst Emission Automatic Roger
MJD	: Modified Julian Date
GPU	: Graphic processing unit
CPU	: Central processing unit
RAM	: Random access memory
GFLOPS	: Giga-floating point operations per second
CUDA	: Compute Unified Device Architecture

CHAPTER 1: INTRODUCTION

1.1 History

Fast radio bursts or FRBs, are bright, broadband pulses of radio emission ranging from milliseconds or less, first discovered while reviewing data in radio pulsar surveys (D. R. Lorimer, Bailes, McLaughlin, Narkevic, & Crawford, 2007). The single pulse (FRB 010724) was detected in a Small Magellanic Cloud survey with the Parkes Telescope in 2001, and had a peak flux density of over 30 Jy and a large dispersive measure, suggesting the existence of a population of bright, extragalactic radio pulses.

This was further strengthened by the detection of four high-dispersion signals in the High Time Resolution Universe survey using the same telescope (Keith et al., 2010). This led to increased searches in new and archived data from the Parkes Telescope, as well as other telescopes such as the Arecibo Telescope (Spitler et al., 2014), the Green Bank Telescope (Masui et al., 2015), the Upgraded Molongo Synthesis Telescope (UTMOST, Caleb et al., 2016), and the Australian Square Kilometre Array Pathfinder (ASKAP, (Bannister et al., 2017)).

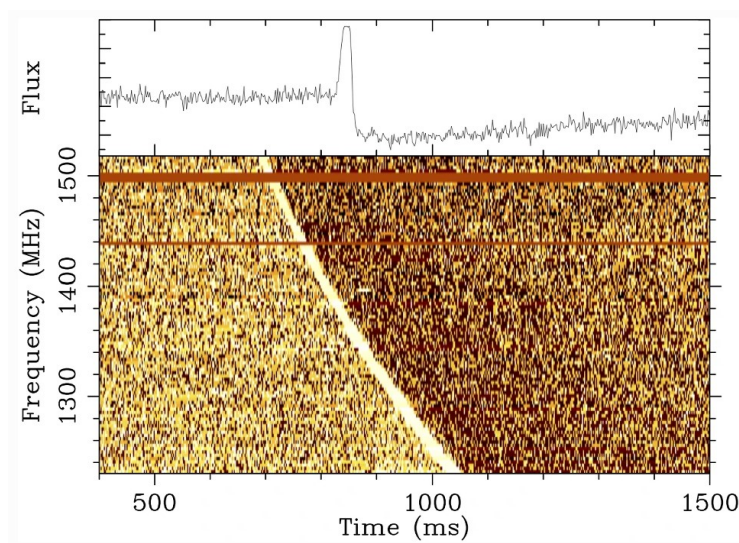


Figure 1.1: Frequency spectrum (bottom panel) and integrated pulse shape (top panel) of the Lorimer burst, the first FRB detected using the Parkes Telescope (D. R. Lorimer et al., 2007).

1.2 Properties of FRBs

FRBs have flux densities around 50 mJy - 100 Jy with widths between 0.8 ms - 5000 ms. There are currently 309 FRB detections so far (Transient Name Server¹ and FRBCAT²) between frequencies 400 MHz to 8 GHz, and 60% of them exhibit repeating patterns e.g. FRB 121102 where a periodicity of 161 days was detected (Cruces et al., 2020). A distinct characteristic of FRBs is their frequency-dependent signal delay which follows the cold-plasma dispersion relation. Dispersion is due to the frequency dependent group velocity of a wave packet when propagating in a dispersive medium. The temporal delay in the FRB signal between two frequencies is given by

$$t = 4.149 \times \text{DM} \left(\nu_{1,\text{GHz}}^{-2} - \nu_{2,\text{GHz}}^{-2} \right) \text{ms}, \quad (1.1)$$

where the dispersion measure (DM) is the column density of free electrons along the line of sight in the unit $\text{cm}^{-3} \text{pc}$ i.e. $\text{DM} \equiv \int n_e dl$ where n_e is the electron density. The DM values observed from FRBs usually exceed the contribution from our galaxy with FRB 160102 having the largest at $\text{DM} = 2596.1 \pm 0.3 \text{ cm}^{-3} \text{pc}$ (Petroff, Hessels, & Lorimer, 2019).

Another characteristic of FRBs are their polarization, and although only a number of them have polarimetric data, results are mixed i.e. some are unpolarized, some either circularly or linearly polarized, and others have both. Linear polarization is parameterized by Faraday rotation measure, RM and from this, the line-of sight magnetic field strength can be obtained, and the results seem close to that of magnetars (W.-Y. Wang, Zhang, Chen, & Xu, 2020). Various other papers have also pointed the origin of several FRBs to the magnetosphere of magnetars (Luo et al., 2020; CHIME/FRB Collaboration et al., 2020)

¹ Transient Name Server (TNS): <https://www.wis-tns.org/>

² FRBCAT: <http://frbcatalog.org/>

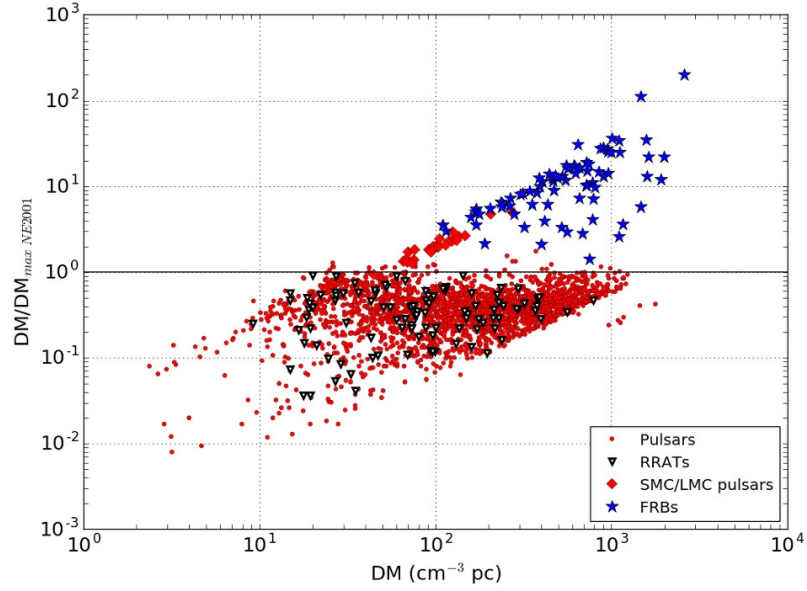


Figure 1.2: Plot of the ratio between the DMs of FRBs, galactic rotating radio transients, pulsars in the Small and Large Magellanic Clouds, and galactic radio pulsars with respect to Milky Way contribution versus their DMs (Petroff et al., 2019).

and the current sample of localized FRB hosts is consistent with magnetar progenitors (Bochenek, Ravi, & Dong, 2021). Magnetars are neutron stars with extremely powerful magnetic fields, up to 10^{15} G. This points to the ‘Decelerating Blast Waves in Magnetars’ model as the FRB progenitor.

1.3 Progenitor and Emission Theories

As stated by Lyubarsky (2014), relativistic blast waves are emitted when restructuring of the magnetar’s core distorts its magnetic field, and the emission is modelled by the synchrotron maser blastwave model, where the blast waves encounter the magnetar’s stationary outer shell, causing forward and reverse shocks (Metzger, Margalit, & Sironi, 2019). The reverse shocks moves the shell and produce coherent synchrotron radiation, which is seen as an FRB, whereas the forward shocks produce an x-ray afterglow, as detected in some multi-wavelength FRB observations (Metzger, Fang, & Margalit, 2020).

Other progenitor theories include mergers such as binary black hole mergers (B. Zhang, 2016), collapses such as dark matter-induced neutron star collapse (Totani, 2013), inter-

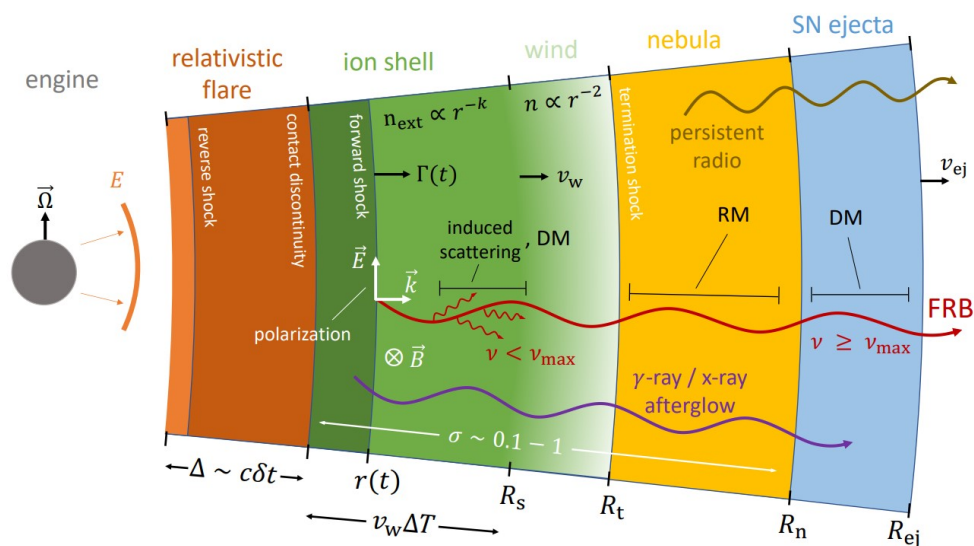


Figure 1.3: Schematic of the production of FRBs as synchrotron maser emission from decelerating relativistic blast waves in magnetars (Metzger et al., 2019).

actions such as neutron star-asteroid belt interaction (Z. G. Dai, Wang, Wu, & Huang, 2016) and theories involving pulsars such as pulsar wind bubbles (Murase, Kashiyama, & Mészáros, 2016). However, all these theories are purely derived from observational basis and are not confirmed. More FRB observational improvements in terms of higher accuracy, multi-wavelength observations and particle detection could narrow it down on the correct theory for FRBs.

1.4 Astrophysical Applications

Aside from searching for the progenitor of FRBs, FRBs also have other significant astrophysical and/or cosmological applications. Examples include:

- Measurement of the Hubble constant via the distance constraint and redshift relation of FRBs (Hagstotz, Reischke, & Lilow, 2021)
- Testing of Einstein’s equivalence principle from the time delay experienced by photons (Wei, Gao, Wu, & Mészáros, 2015; Reischke, Hagstotz, & Lilow, 2021)
- Bounding of photon rest mass using kinematic analysis of light propagation (Wu et al., 2016; H. Wang, Miao, & Shao, 2021)

- Constraining the epoch of reionization using highly dispersed FRBs (Pagano & Fronenberg, 2021)
- Revealing hidden baryons in the Universe using dispersion of localized FRBs (Macquart et al., 2020)
- Constraining the equation of state of dark energy and other cosmological parameters using DM-redshift relation (Zhou, Li, Wang, Fan, & Wei, 2014)
- Measurement of turbulence of cosmic web/intergalactic medium (IGM) from polarization measurements (Ravi et al., 2016)
- Reconstruction of baryon fraction in the IGM from DM angular power spectrum (J.-P. Dai & Xia, 2021)
- Constraining galaxy haloes using dispersion and scattering of FRBs (Ocker, Cordes, & Chatterjee, 2021)

1.5 Objectives

The objectives of this project are:

- To understand FRB detection methods
- To develop a program that independently searches for FRBs in radio telescope data
- To compare performance of the program developed with BEAR
- To test the performance increase for GPU dedispersion

This thesis is organized in the following manner. Chapter 2 looks at literature on available FRB detection methods, data analysis, and instrumentation involved. Chapter 3 briefs on the flow of the project and explains the methodology involved in the program as well as testing methods. Chapter 4 presents the results of the test. In Chapter 5, discussions regarding the program's performance is made. Finally, the summary of this project is described in Chapter 6.

CHAPTER 2: LITERATURE REVIEW

2.1 Instrumentation

To observe FRBs, both single dish telescopes and interferometry techniques are used. Single dishes like the Parkes Telescope, Green Bank Telescope and the Five-hundred-meter Aperture Spherical Telescope (FAST) are used due to their high sensitivity, allowing for accurate flux readings, but suffer from large location uncertainty (Keane et al., 2016). On the other hand, interferometry allows for higher resolution and are much more versatile as these can perform fly's eye survey (Shannon et al., 2018) allowing for a much higher detection area. However, they are computationally expensive and inefficient for real time tracking. In practice, both are used in FRB detection to utilise their advantages e.g. single dishes would first detect the FRB, and its source is localized using interferometry techniques (Marcote et al., 2020).

FRB searching or observations are usually done blind where radio telescopes would observe a large portion of the sky over a certain period of time (Keane & SUPERB Collaboration, 2017). However, recently some observations are made near hosts of soft gamma-ray bursts i.e. large bursts of gamma rays and X-rays, which are also known as soft gamma repeaters or SGR (Madison et al., 2019; Katz, 2020). This is because SGRs have been conjectured to be from magnetars, and as stated earlier, are also one of the leading hypothesis for FRBs.

2.2 Data Analysis

Previously, FRB data from radio telescopes are detected and/or analysed using pulsar signal processing programs such as SIGPROC and PRESTO, based on methods that search for new pulsar candidates. Currently, there are many FRB searching softwares such as HEIMDALL and BEAR, and they are mainly based on the matched filter, quoted

as the *most powerful statistics* for detecting signals with a priori waveform (Vainshtein & Zubakov, 1970) and are performed based on the methods underlined in Cordes & McLaughlin, 2003. Most FRB data analysis programs have a similar flow, starting with the input which is a binary data file called filterbanks (D. Lorimer, 2007). The data is then passed through RFI removal/mitigation. Strong RFI are removed by masking contaminated frequency channels, whereas weaker RFI are removed by subtracting the interference modulation spectrum i.e. Fourier transform of zero-DM spectrum (Ransom, n.d.; Kocz, Briggs, & Reynolds, 2010) or using zero-DM matched filter (Men et al., 2019). Then, the program performs dedispersion at different DMs, using various optimization algorithms such as the tree algorithm, subband dedispersion and/or using CPU or GPU parallelization (Magro et al., 2011; Barsdell, Bailes, Barnes, & Fluke, 2012). The program then applies the matched filter to the dedispersed data, for which the peaks are reported as FRB candidates. The candidates are then passed through candidate grouping i.e. clustering of candidates of the same event (Pang, Goseva-Popstojanova, Devine, & McLaughlin, 2018), and through filters corresponding to parameters such as their DM (only signals with large DMs are considered as FRBs), SNR (only signals with SNR above a certain threshold), pulse width, and for multi-beam receivers, the number of beams detected (large number of detection beams may be due to terrestrial sources). Finally, the results are manually examined to confirm the signal is an FRB i.e. depending on the presence of the dispersive sweep in the non-dedispersed data (Rane et al., 2015).

2.3 Pipelines

With the ever increasing number of telescopes used to observe FRBs, the data obtained exponentially increases, presenting researchers with the situation known as ‘data avalanche’. Therefore, to quickly filter through the data, pipelines i.e. automatic sequencing of programs are used to detect and analyze FRBs in telescope data, outputting FRB

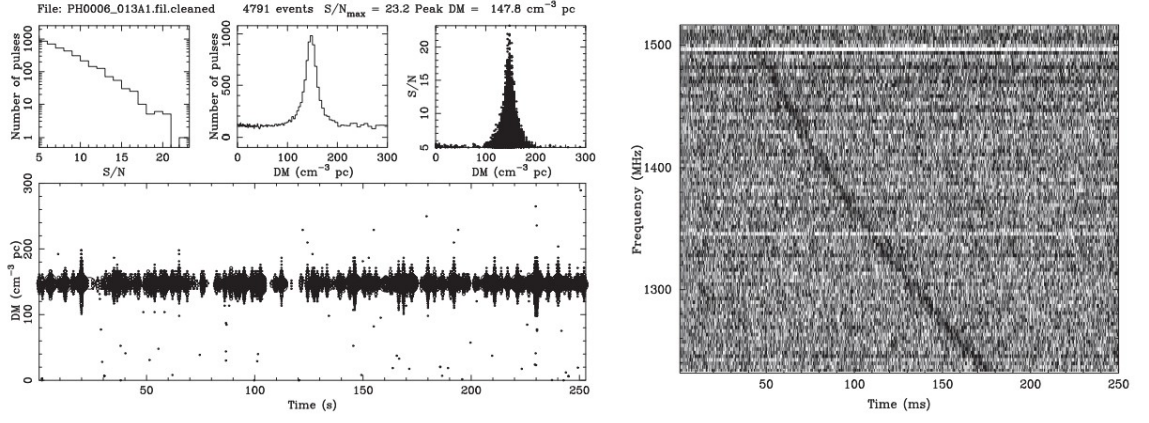


Figure 2.1: Output of PRESTO’s pulse processing pipeline for single pulse from PSR J0837-4135. The non-dedispersed spectrum (right plot) displays a noticeable dispersive sweep, corresponding to a large DM (Rane et al., 2015).

candidates (Petroff et al., 2019). Along with the previously stated processes, pipelines also include DM refining using repetitive dedispersion and SNR search, as well as localization using SNR sky maps. Pipeline are often independently develops for specific telescopes to efficiently make use of their corresponding survey parameters. Examples of FRB detection/analysis pipelines include:

- Westerbork Telescope: AMBER which utilizes multi-core GPU computation and real time detection (Sclocco, Heldens, & van Werkhoven, 2020).
- CHIME/FRB: ‘bonsai’ algorithm i.e. a more efficient tree dedispersion algorithm, and Apache Airflow and Docker based analysis pipeline to automatically schedule processes (CHIME/FRB Collaboration et al., 2018; Michilli et al., 2021).
- Arecibo Telescope: PALFA Single-pulse Pipeline based on PRESTO’s single pulse search (Patel et al., 2018).
- MeerKAT: MeerTRAP which uses both coherent mode where multiple beams are interfered for localization and incoherent mode where beams are summed over for a large field-of-view (Sanidas et al., 2017).
- ASKAP: CRAFT which utilizes fly’s eye survey using each dish independently, and the FREDDA algorithm (James et al., 2019).

CHAPTER 3: METHODOLOGY

3.1 Flow of the project

Figure 3.1 shows the flowchart of the development of the entire project. The project started with literature review to understand the basic concepts for FRBs such as their properties and progenitor theories, as well as theories regarding available FRB detection methods and pipelines used on various radio telescope. Then, I proceeded to explore pulsar and transient analysis programs such as SIGPROC and PRESTO in order to understand basic processes in radio telescope data processing. I also gathered FRB data from radio telescopes used in previous researches, as well as develop a code to generate fake FRB data. Next, I learned and explored BEAR to understand more on the processes regarding FRB data analysis, as well as tested it with the available data. With that, I then developed the independent FRB detection program, and tested it out similarly. After that, the program's performance was analyzed and compared with BEAR, and finally, GPU implementation was tested out, specifically for dedispersion.

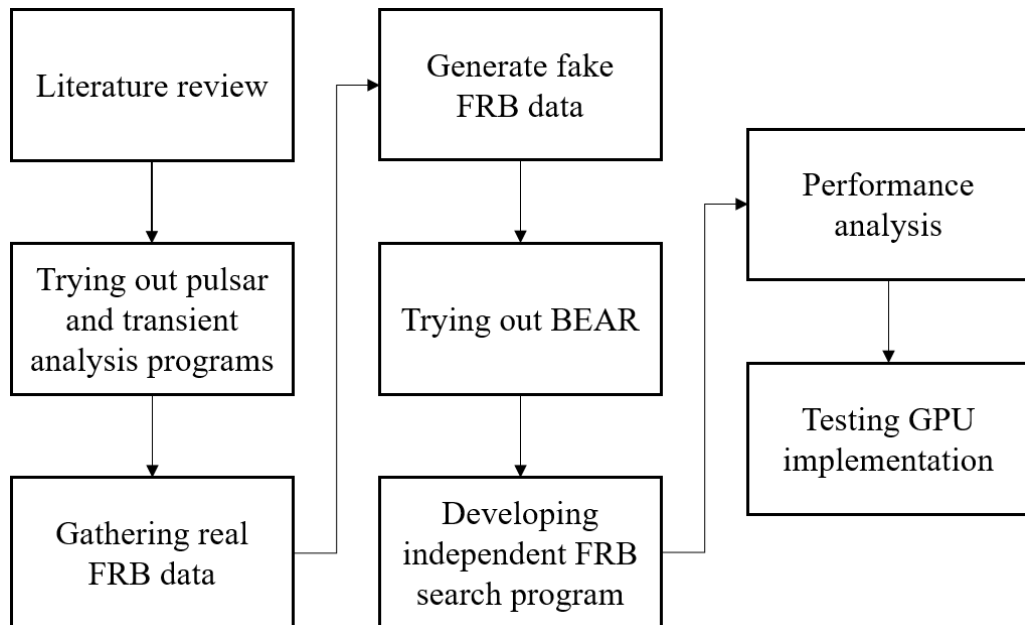


Figure 3.1: Flowchart of the development of the project.

3.2 Introduction to PoLaR BEAR

This independent FRB searching program is developed based on the Burst Emission Automatic Roger (BEAR), as demonstrated in Men et al., 2019, which is an FRB searching pipeline mainly written in C++ (with some Fortran and Python), and utilizes many pulser/radio transients searching programs such as SIGPROC, PRESTO, CFITSIO, PSRCAT, PSRCHIVE, TEMPO, and TransientX. This project uses Python due to:

- Relatively modern language;
- Easily understood and modified by beginners and advanced users;
- Indexing style of operation for functions rather than performing loops; and
- Ability to utilize and handle multidimensional arrays.

This program will also be standalone, requiring only a few general Python packages. This program will be referred to as the ‘PythOn LAnguage Radio Burst Emission Automatic Roger’ or PoLaR BEAR. Shown in Figure 3.2 is the block diagram/flowchart for the procedures in PoLaR BEAR. The following sections will explain each procedure in detail.

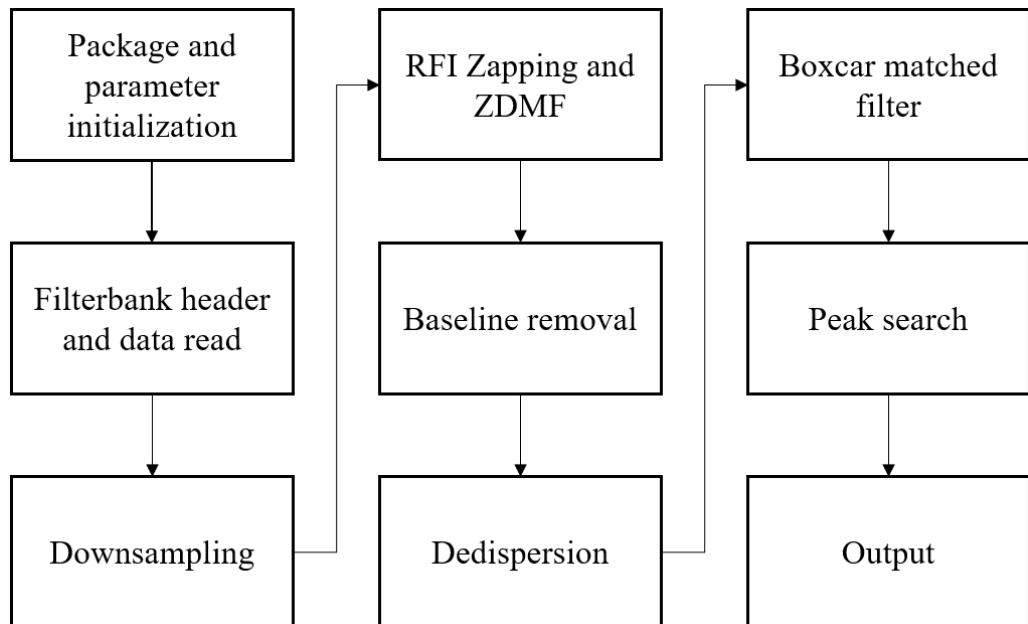


Figure 3.2: Block diagram for procedures in PoLaR BEAR.

3.3 Initialization

The first section of the program involves the initialization of the required packages:

1. Numpy: Handles mathematical functions and multidimensional single data type arrays,
2. Struct and Bitarray: Handles and operates on binary data types,
3. Matplotlib: Plotting of data, analysis output, etc.
4. Tabulate: Formatting the output in table form.

Analysis parameters are also defined here.

Then, the data is read. The type of radio telescope data that are used are called filterbanks, which are binary data files (D. Lorimer, 2007). These files consists of two parts; header and data. The header stores the parameters of the data e.g. telescope ID, machine ID, source name, the sky coordinates the telescope is pointing towards, start time of the data, sampling time, frequency channels, polarization channels, and the number of bits of the data. The data then consists of correlated and integrated voltage data from the radio telescope's receiver, arranged in time, polarization channels and frequency channels. The program reads the header to a Python dictionary, and the data to a bytearray object. To reduce memory usage, the data is slice using bitarray indexing based on the set start and end times. Finally, the data is converted into a 64-bit Numpy float 2-D array.

3.4 Pre-analysis

After the data is extracted, the next part is the pre-analysis i.e. the preparation of the data before further analysis. First, the program performs downsampling where the data is summed every certain number of samples to reduce the time resolution of the data. Here `numpy.add.reduceat` is utilized i.e. performing local addition with specified slices. This is done also to reduce the size of the data as well the computation cost.

Then, the program performs RFI mitigation. Here two methods are used; zapping RFI and the zero-DM matched filtering or ZDMF for short. Zapping RFI is to remove the data from the frequency channels contaminated with RFI, which is a very common measure in radio astronomy e.g. signals at 1.55 GHz due to RFI from satellite communication (C. F. Zhang et al., 2021). Then, ZDMF is performed, where narrow band RFI with no dispersive measure is removed (Men et al., 2019). The program starts by estimating the zero-DM time series by summing the data over all the temporal domain, denoted as $\mathbf{s}_{\text{DM}=0}$. Then, the residual of fitting the zero-DM waveform to every channel is reduced into

$$\chi^2 = (\mathbf{s}_i - \alpha_i \mathbf{s}_{\text{DM}=0} - \beta_i)^2 \quad (3.1)$$

where α_i is the scale factor given as

$$\alpha_i = \frac{\mathbf{s}_{\text{DM}=0} \cdot \mathbf{s}_i - \frac{1}{N} \sum \mathbf{s}_i \sum \mathbf{s}_{\text{DM}=0}}{\mathbf{s}_{\text{DM}=0} \cdot \mathbf{s}_{\text{DM}=0} - \frac{1}{N} \sum \mathbf{s}_{\text{DM}=0} \sum \mathbf{s}_{\text{DM}=0}} \quad (3.2)$$

and β_i is the baseline (not considered here as it does not affect pulse detection). Therefore, the RFI is removed from the data by obtaining the new time series at the i -th channel using

$$\mathbf{s}'_i = \mathbf{s}_i - \alpha_i \mathbf{s}_{\text{DM}=0} \quad (3.3)$$

Shown in Figure 3.3 is an example of the usage of ZDMF on generated FRB data with a narrow-band RFI over a short duration.

The final step before the analysis is to perform baseline removal i.e. calibrating the data in every channel to have equal averages. For frequency channels with non-zero mean, the

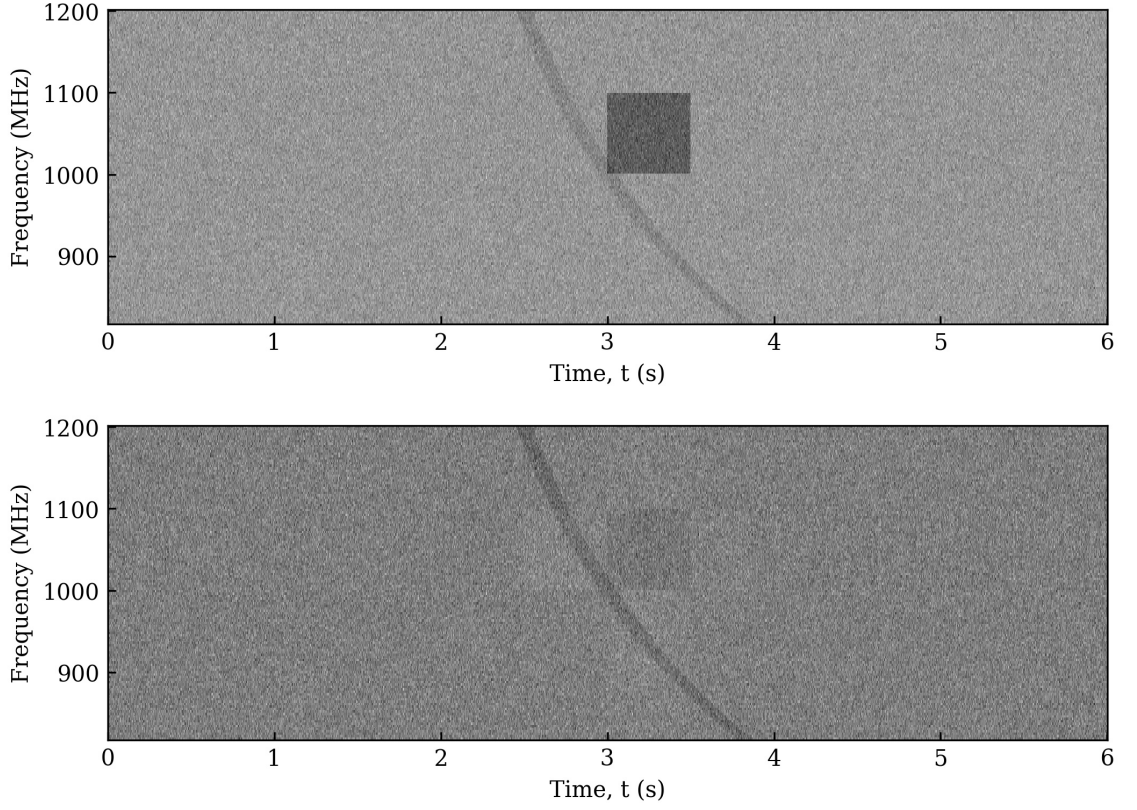


Figure 3.3: Frequency spectrum of generated FRB data at $DM = 400 \text{ cm}^{-3} \text{ pc}$ with a narrow-band RFI over a short duration, before (upper) and after zero-DM matched filter (lower).

new time series at the i -th channel is

$$\mathbf{s}'_i = \mathbf{s}_i - \bar{\mathbf{s}}_i \quad (3.4)$$

3.5 Analysis

After the pre-analysis is complete, the program continues the analysis by performing three operations; dedispersion, boxcar matched filter, and pulse search. Dedispersion is performed to remove the time delay due to the cold-plasma dispersion, so that the pulse occur at the same time in all frequency channels. This is done by calculating the delay for every channel using Equation 1.1, and then shifting the data in the time axis based on that delay, in this case using `numpy.roll`. Figure 3.4 shows an example of dedispersion performed on FRB data. Summing over all the frequency channels gives the pulse profile

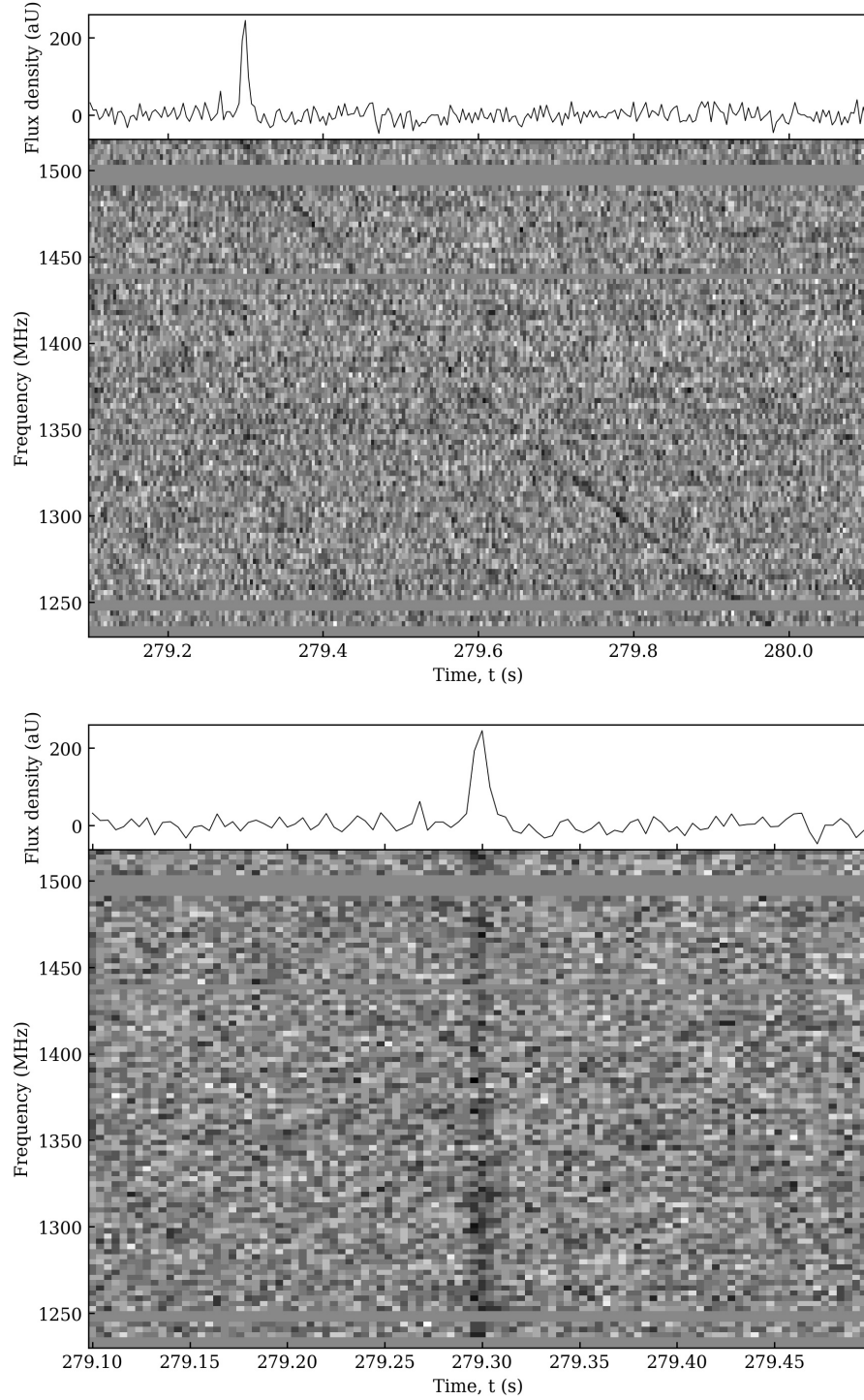


Figure 3.4: Frequency spectrum and pulse profile for data from FRB 010621 before (upper) and after (lower) dedispersion at $748 \text{ cm}^{-3} \text{ pc}$.

of the FRB. For an FRB data with unknown DM, the data is dedispersed at many trial DMs, producing a set of profiles, which is referred to as 1-D dedispersed time series.

The second operation is the boxcar matched filter. This process searches for burst signals in the dedispersed time series using a matched filter. Here it is assumed that

the FRB can be approximated by a square wave shape, hidden in Gaussian noise. The template of the filter for an FRB with amplitude, pulse center and width of A , t_0 , and W respectively, is given by

$$h(t, t_0, W) = \begin{cases} A, & \text{if } |t - t_0| \leq W/2, \\ 0, & \text{otherwise} \end{cases} \quad (3.5)$$

The concept that is used here to find the burst is called the likelihood ratio test, quoted as the ‘most powerful test’ (Fisz, 1963). The key is the detection statistic S defined as the logarithmic likelihood ratio between the cases of having and not having the signal i.e.

$$S \equiv \frac{\Lambda_{\text{Sig}}}{\Lambda_{\text{Null}}} = \frac{\mathbf{s}^2 - (\mathbf{s} - \mathbf{h})^2}{2\sigma^2} \quad (3.6)$$

where σ is the standard deviation of the noise present, assuming it is Gaussian noise.

With the filter established in Equation 3.5, Equation 3.6 reduces to

$$S = \frac{1}{N_{\text{box}}\sigma^2} \left(\sum_{|t-t_0| \leq W/2} s(t) \right)^2 \quad (3.7)$$

where N_{box} is the number of data points in the burst. This is directly related to the SNR of the burst i.e. $\text{SNR} = \sqrt{S}$.

To perform this, the boxcar filter is produced for a certain pulse width and is convolved with a time series at a certain DM. Convolution is defined as an integral that expresses the amount of overlap of two functions as they are shifted over each other i.e.

$$(f * g)(t) = \int_{-\infty}^{\infty} f(t)g(t - \tau) d\tau \quad (3.8)$$

In this case, both $s(t)$ and $h(t)$ are discrete, allowing the integral to be changed into a summation for all t_0 ,

$$(s * h)(t_0) = \sum_{t=-\infty}^{\infty} s(t_0)h(t_0 - t) \quad (3.9)$$

which would produce the summation term in Equation 3.7 at all t_0 in the data.

Here, `numpy.convolve` is used to perform convolution. This produces a 1-D array of S values for all possible pulse epoch in the data. Extending this to different pulse widths and time series at different DMs gives a 3-D array of S at for different t_0 , DM and W, which is referred to as an S-cube.

The final step in the analysis is to perform a peak search and clustering of candidates in the S-cube. Peaks in the S-cube which are more than a certain threshold, γ_0 (usually $\gamma_0 \approx 42$) denotes an FRB candidate detection at a certain t_0 , DM and W. To apply this, the program starts by searching for the maximum in the S-cube. If it is larger than the threshold, the program performs a neighbor search. The neighbour search inspects a region around the peak; if it matches that of a monotonically decreasing function, they are removed from the search. This is done so that other bright candidates near the peak are not shadowed. Then, the neighbours of the removed region are checked as well, until the values are lower than the threshold. This ensures the suppression of duplicate candidates. The peak is then reported as a candidate, and the search continues until all the remaining values are lower than the threshold.

Note that for a threshold of γ_0 , there is a non-zero false alarm probability i.e. false detection due to statistical fluctuation. For pure Gaussian noise, the false alarm probability is given by (Men et al., 2019)

$$P_{\text{FA}} = \text{erfc} \left(\sqrt{\frac{\gamma_0}{2}} \right) \simeq \sqrt{\frac{2}{\pi \gamma_0}} e^{-\gamma_0/2} \quad (3.10)$$

3.6 Output

The final section deals with the output. There are 4 types of outputs:

- Main analysis plot: A complete summary plot similar to that of the original BEAR as shown in Figure 3.5. Consists of a waterfall data plot, S-cube colourmesh plots (DM vs t , W vs DM), S-cube plots (vs t , W , DM), highlights of the candidates (position in S-cube and in waterfall plot), and the pulse profile as well as the frequency profile of the best candidate i.e. maximum of the S-cube.
- Candidates' pulse profile plots: Plots of the dedispersed time series at DMs of the candidates as shown in Figure 3.6.
- Candidates' analysis plots: Detailed plots of each candidates' analysis as shown in Figure 3.7. Detailed plots of each candidates' analysis. Consists of the pulse profile, dedispersed waterfall plot, frequency profile, localized S-cube colourmesh plots (DM vs t , W vs DM) and S-cube plots (vs W , DM).
- Analysis properties and results: A text file of the analysis parameters used and the properties of the candidates as shown in Figure 3.8.

The plots are handled using `matplotlib.pyplot.subplots`, and the analysis properties and results text are formatted using `tabulate`.

Source: G051.7-54.8, Time (MJD): 55612.077997685184528

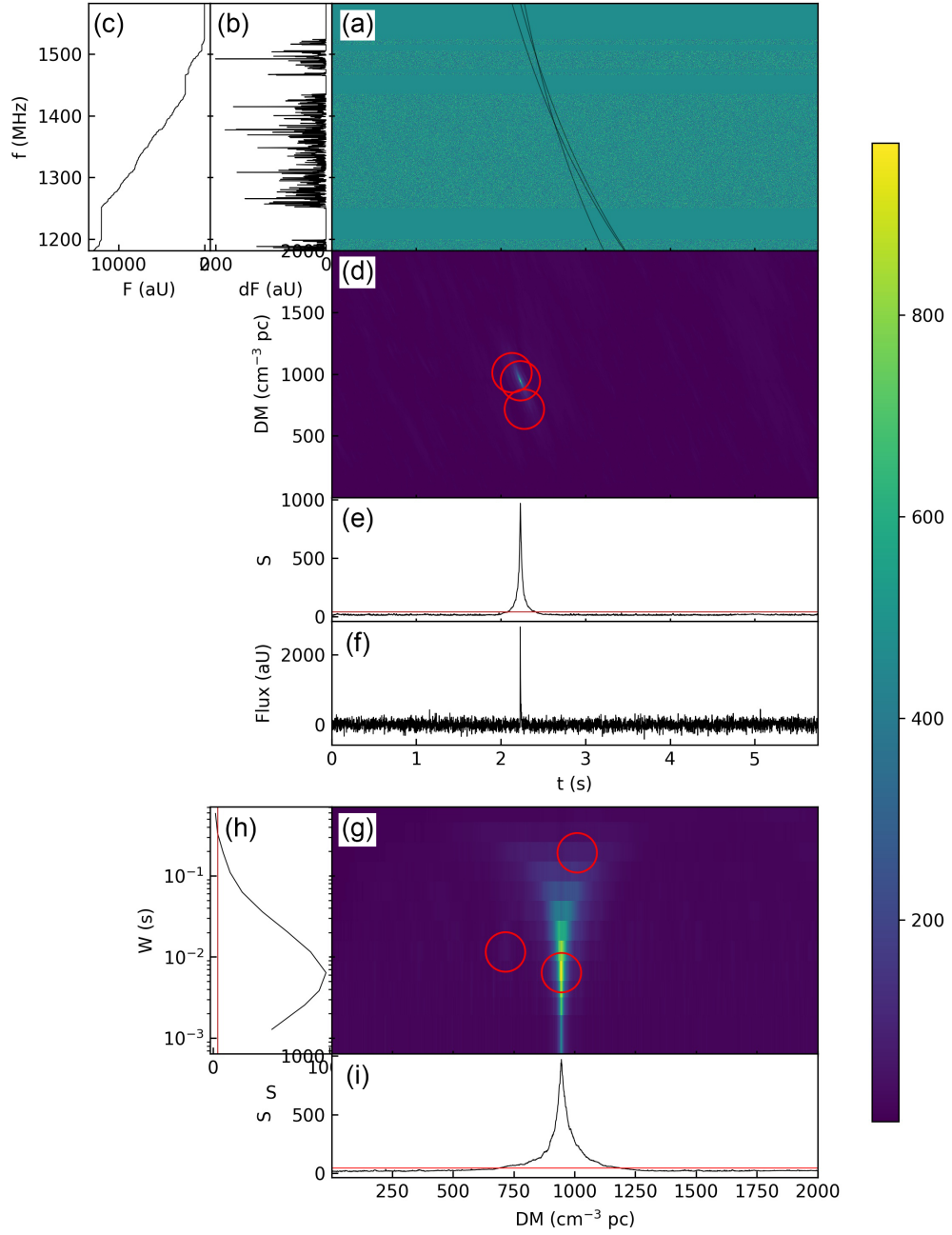


Figure 3.5: Example PoLaR BEAR main analysis plot for FRB 110220. Consists of (a) filterbank data, (b) frequency profile of first candidate, (c) integrated frequency profile of first candidate, (d) S as a function of DM and time, (e) S as a function of time, (f) pulse profile of first candidate, (g) S as a function of W and DM, (h) S as a function of W , and (i) S as a function of DM.

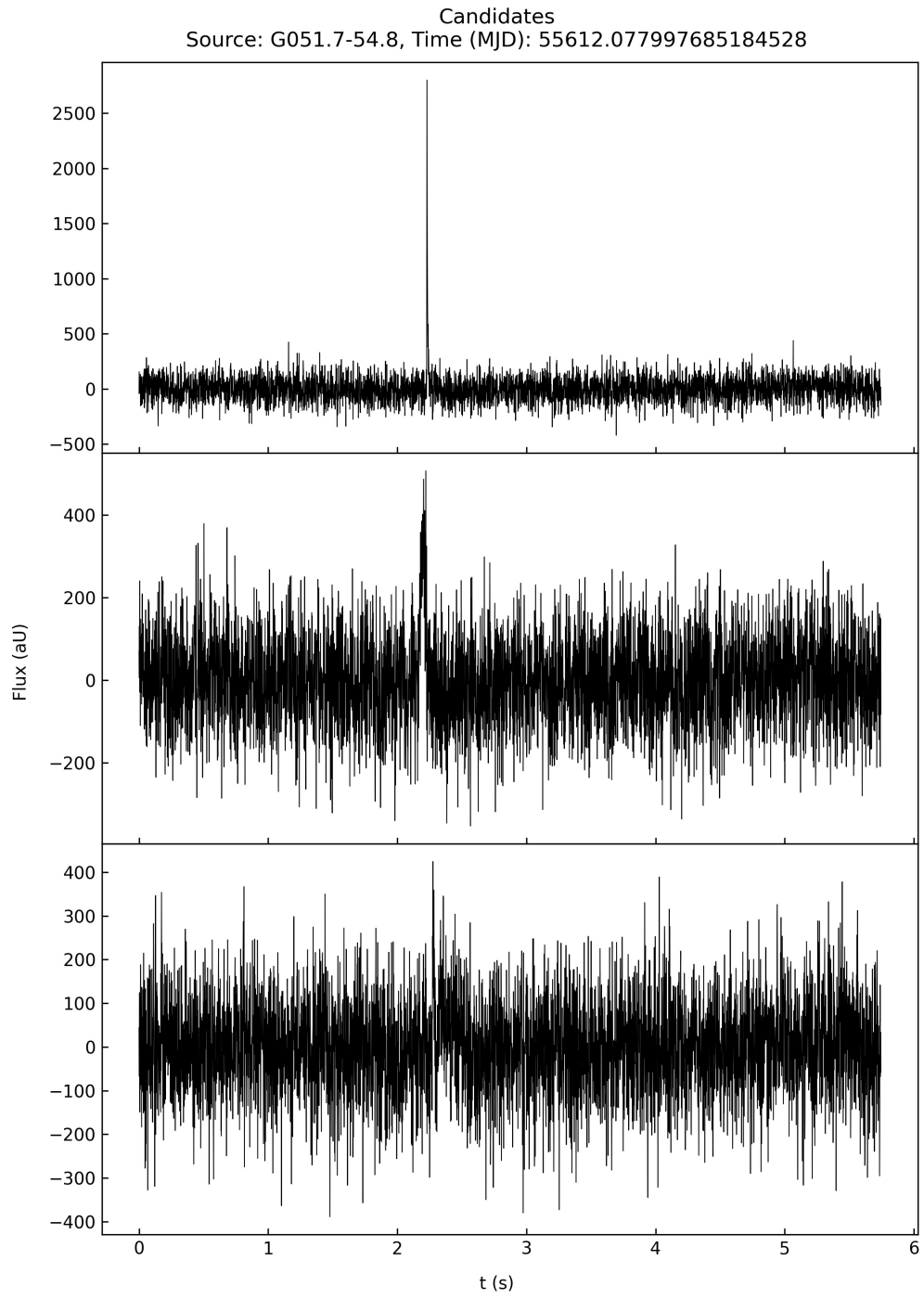


Figure 3.6: Example PoLaR BEAR candidates' pulse profile plots for FRB 110220.

Candidate 1, DM = 946.00 $\text{cm}^{-3} \text{ pc}$
Source: G051.7-54.8, Time (MJD): 55612.077997685184528

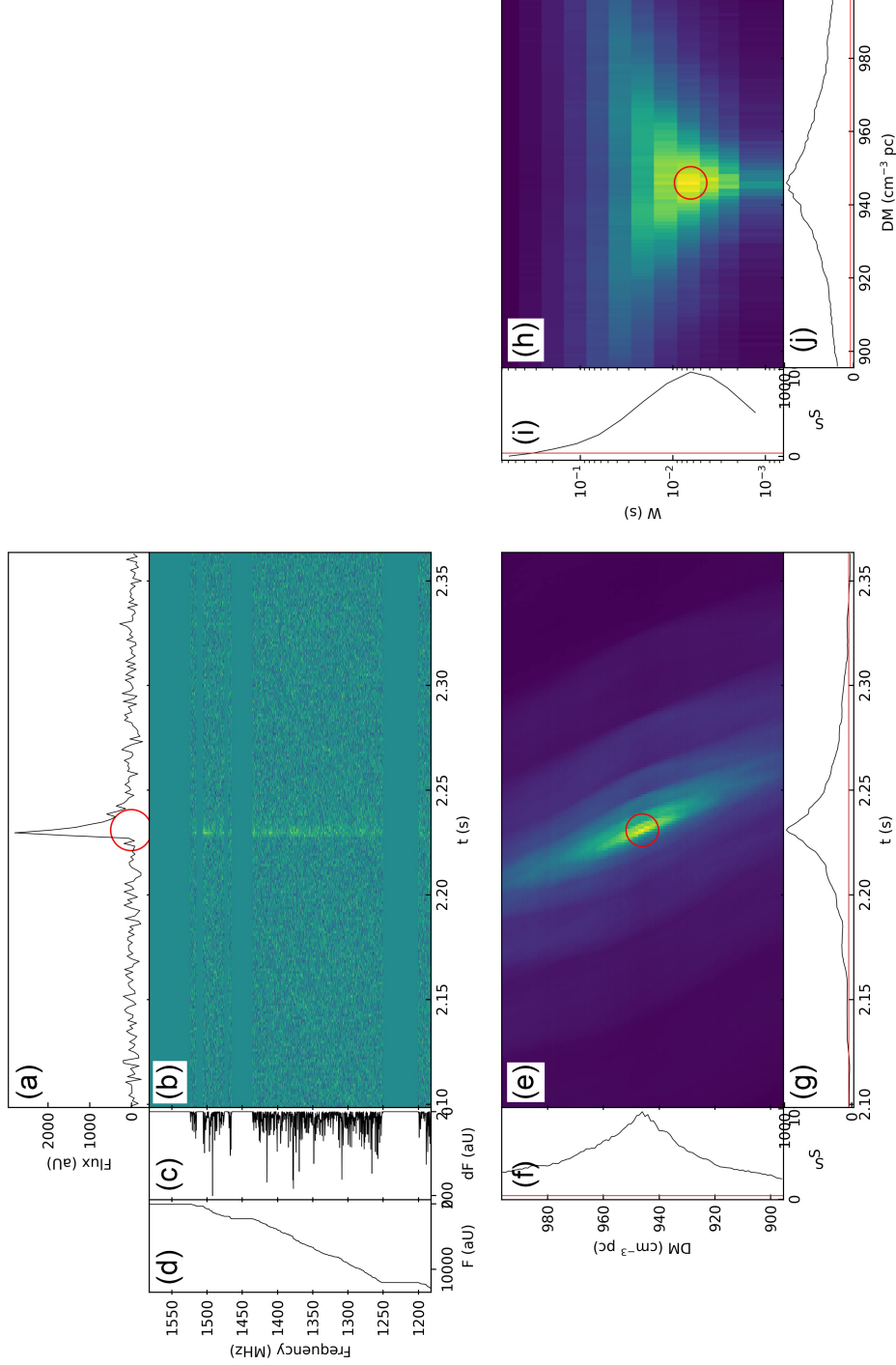


Figure 3.7: Example PoLaR BEAR candidates' analysis plot for FRB 110220. Consists of (a) pulse profile of the candidate, (b) dedispersed filterbank data, (c) frequency profile of the candidate, (d) integrated frequency profile of the candidate, (e) S as a function of DM and time, (f) S as a function of DM, (g) S as a function of time, (h) S as a function of W and DM, (i) S as a function of W, and (j) S as a function of DM.

Source: G051.7-54.8
Time (MJD): 55612.077997685184528

Downsampling coefficient: 20
Start: 0.72000000
End: 0.74000000
Threshold: 41.99597534

Zapped frequencies:
1200.00 - 1250.00 MHz
1435.00 - 1465.00 MHz
1470.00 - 1475.00 MHz
1505.00 - 1515.00 MHz
1524.00 - 1600.00 MHz

Candidate	DM (cm-3 pc)	Width (s)	Time (s)	S	SNR
1	946	0.0064	2.23104	970.687	31.1559
2	1011	0.192	2.13248	70.8987	8.42014
3	716	0.01152	2.2784	43.0642	6.56233

Figure 3.8: Example PoLaR BEAR analysis properties and results for FRB 110220. Includes the source name, start time of the data in MJD, downsampling coefficient, start and end percentage, threshold for S, zapped frequency range, and the candidates' properties e.g., DM, width, pulse time, S, and SNR.

3.7 PoLaR BEAR Tests

To test PoLaR BEAR, two types of data are used; real FRB data and generated FRB data. The FRB properties obtained from PoLaR BEAR are compared with the actual measured/generated properties, as well as comparing them to the original BEAR's output.

3.7.1 Real FRB data

Here, publicly released FRB data from various radio telescopes are used, mainly the Parkes Telescope, with some from Lovell Telescope, and STARE2, consisting of the Owens Valley Radio Observatory, Goldstone Observatory, and Delta. The properties of the FRBs used are as shown in Table 3.1. The frequency channels contaminated with RFI were inspected visually and zapped accordingly.

Table 3.1: Properties of the real FRB data used for PoLaR BEAR tests. The true properties are taken from TNS and FRBCAT.

Telescope	FRB Name	Start time (MJD)	File name (Beam)	DM (cm^{-3} pc)	W (ms)	SNR
Parkes ^a	FRB 010124	51934.019976851850515	BJ0009_02551.fl (5)	790.3	10.6	10.6
Parkes ^a	FRB 010621	52081.539953703701030	PM0141_017A1.fl (10)	745	7	16.3
Parkes ^a	FRB 010724	52114.806423611109494	SMC021_00861.fl (6)	375	20	100
Parkes ^b	FRB 090625	55007.910081018519122	2009-06-25-21_50_31.fl (6)	899.55	1.92	30
Parkes ^a	FRB 110220	55612.077997685184528	2011-02-20-01_52_19.fl (3)	944.38	6.59	54
Parkes ^a	FRB 110626	55738.896585648144537	2011-06-26-21_31_05.fl (12)	723	1.41	12
Parkes ^a	FRB 110703	55745.790069444446999	2011-07-03-18_57_42.fl (5)	1103.6	3.9	17
Parkes ^a	FRB 120127	55953.339050925926131	2012-01-27-08_08_14.fl (4)	553.3	1.21	13
Parkes ^b	FRB 121002	56202.547638888885558	2012-10-02-13_08_36.fl (12)	1629.18	5.44	16
Parkes ^b	FRB 130626	56469.620752314811398	2013-06-26-14_53_53.fl (1)	952.4	1.98	21
Parkes ^b	FRB 130628	56471.164502314815763	2013-06-28-03_56_53.fl (5)	469.88	0.64	29
Parkes ^b	FRB 130729	56502.375752314816054	2013-07-29-09_01_05.fl (10)	861	15.61	14
Parkes ^c	FRB 140514	56791.712291666663077	2014-05-14-17_05_42.fl (1)	561.7	2.816	16
Parkes ^d	FRB 150215	57068.853564814817219	2015-02-15-20_29_08.fl (13)	1105.6	2.88	19
Lovell ^e	FRB 121102	57798.871967592596775	57798_73718_J0532+3305_000027.fl	557	3	14
STARE2 (OVRO) ^f	FRB 200428a	58967.230011574070002	candidate_ovro_20200428.fl	332.702	0.61	21
STARE2 (GDSCC) ^f	FRB 200428b	58967.300127314819999	candidate_gdscc_20200428.fl	332.702	0.61	15
STARE2 (Delta) ^f	FRB 200428c	58967.237430555560000	candidate_delta_20200428.fl	332.702	0.61	20

^a: <https://data-portal.hpc.swin.edu.au/dataset/parkes-frbs-archival-data>

^b: <https://data-portal.hpc.swin.edu.au/dataset/fast-radio-burst-data-high-time-resolution-universe-survey-high-latitude>

^c: <https://data-portal.hpc.swin.edu.au/dataset/fast-radio-burst-data-frb-140514>

^d: <https://data-portal.hpc.swin.edu.au/dataset/fast-radio-burst-data-frb-150215>

^e: <https://zenodo.org/record/3974768#.YGWzqK8zap0>

^f: <https://data.caltech.edu/records/1647>

3.7.2 Generated FRB data

Another way to test the data is by producing a simulated FRB data, or commonly known as ‘Fake’ data. To produce the data, a simple Python code is used, based on SIGPROC’s Fake (D. Lorimer, 2007), which produces fake pulsar data which are used to test pulsar detection pipelines.

The program first randomly selects the width, SNR, and DM of the generated FRB from a set range. The SNR is scaled based on Equation 3.6, where the channel SNR is given by

$$\text{SNR}_i = \sqrt{\frac{N_{\text{chans}} W}{t_{\text{samp}}}} \quad (3.11)$$

where N_{chans} is the number of frequency channels and t_{samp} is the sampling time. Then, the dispersion delay is calculated using Equation 1.1. The program then passes through all the observation time of the data. If the time (with the dispersion delay considered) is in the pulse window, the data is set to SNR_i . Lastly, Gaussian noise is added to the entire data using `numpy.random.normal`. The program then outputs the data as a filterbank, with corresponding parameters in the header.

50 fake FRB data was generated, with a sampling time of 64 μs for 30 seconds observation time, 512 frequency channels with a 1200 MHz first channel and 0.1 MHz bandwidth. The fake FRBs are generated with widths between 0.5 to 5 ms, SNR between 8 and 50, and DMs between 200 and 1900 $\text{cm}^{-3} \text{pc}$. The properties of the generated fake FRBs are as shown in Table 3.2.

Table 3.2: Properties of the Fake FRB data used for PoLaR BEAR tests.

Fake	File name	DM (cm^{-3} pc)	W (ms)	SNR	Fake	File name	DM (cm^{-3} pc)	W (ms)	SNR
1	fake_output0.fl	566.158	3.47103	34.1301	26	fake_output25.fl	1358.91	4.79527	18.5694
2	fake_output1.fl	1476.21	3.97177	46.3679	27	fake_output26.fl	480.351	2.97478	42.4061
3	fake_output2.fl	1858.64	2.57209	26.5634	28	fake_output27.fl	1668.8	2.42997	29.9655
4	fake_output3.fl	399.97	2.77513	10.1587	29	fake_output28.fl	359.856	4.1512	31.7901
5	fake_output4.fl	573.649	0.710951	16.1083	30	fake_output29.fl	426.874	1.36033	28.9338
6	fake_output5.fl	1187.42	3.8433	34.5618	31	fake_output30.fl	1308.65	2.71006	11.783
7	fake_output6.fl	1028.33	1.66997	42.8729	32	fake_output31.fl	352.708	0.863634	28.142
8	fake_output7.fl	1337.1	3.16891	45.5356	33	fake_output32.fl	745.125	0.82552	32.431
9	fake_output8.fl	1364.17	2.16554	15.2655	34	fake_output33.fl	1355.43	2.69499	34.6861
10	fake_output9.fl	1321.39	4.92548	33.4504	35	fake_output34.fl	741.125	2.97293	11.9684
11	fake_output10.fl	1666.28	3.77166	44.4121	36	fake_output35.fl	1046.19	3.98829	18.2477
12	fake_output11.fl	728.46	2.61624	20.7568	37	fake_output36.fl	1199.7	1.4724	17.7535
13	fake_output12.fl	789.509	1.77699	44.6985	38	fake_output37.fl	518.282	4.72503	49.626
14	fake_output13.fl	1744.95	4.58435	37.8006	39	fake_output38.fl	1799.01	4.07805	23.5333
15	fake_output14.fl	1530.5	1.14656	47.1532	40	fake_output39.fl	670.819	2.36506	19.3561
16	fake_output15.fl	742.392	3.77817	26.9581	41	fake_output40.fl	1688.62	0.997483	40.5665
17	fake_output16.fl	1504.54	3.39606	9.8772	42	fake_output41.fl	1195.6	1.85354	30.0239
18	fake_output17.fl	669.927	2.79792	11.7874	43	fake_output42.fl	1869.7	1.82071	24.1694
19	fake_output18.fl	1287.46	1.60874	9.00864	44	fake_output43.fl	587.108	3.61604	11.8553
20	fake_output19.fl	669.849	3.16439	23.6871	45	fake_output44.fl	601.626	4.16235	33.3841
21	fake_output20.fl	1395.44	4.48013	39.7673	46	fake_output45.fl	746.818	2.50385	9.14934
22	fake_output21.fl	678.089	2.73084	21.4789	47	fake_output46.fl	1268.11	1.02883	15.4958
23	fake_output22.fl	393.089	2.40809	35.0218	48	fake_output47.fl	1818.44	4.73783	40.2606
24	fake_output23.fl	848.94	2.227	17.862	49	fake_output48.fl	1734.89	2.3775	40.4545
25	fake_output24.fl	846.969	1.62728	33.0218	50	fake_output49.fl	917.338	3.38351	40.1697

CHAPTER 4: DATA ANALYSIS AND RESULTS

Here the results of the tests are presented. First, the parameters detected using PoLaR BEAR and BEAR are shown and compared to the true parameters. Second, the difference between the detections and the true parameters are observed, and the accuracy of the outputs of PoLaR BEAR and BEAR are compared to characterize the performance of PoLaR BEAR.

4.1 Real FRB data

PoLaR BEAR was able to detect all 19 FRBs in all real FRB files. As a comparison, the original BEAR was only able to detect 14 out of 19 FRBs. The non-detections were from FRB 130729, FRB 140514, and the three FRB 200428 data due to small pulse widths, relatively low SNR, and updated header formatting respectively, for which the latter was easily overcome in PoLaR BEAR by adding them to the dictionary. The detected DM, W, and SNR for PoLaR BEAR and BEAR for each of the real FRBs are as shown in Table 4.1.

Table 4.1: Detection results for real FRB data using PoLaR BEAR and BEAR.

FRB	True DM (cm^{-3} pc)	PoLaR DM (cm^{-3} pc)	BEAR DM (cm^{-3} pc)	True W (ms)	PoLaR W (ms)	BEAR W (ms)	True SNR	PoLaR SNR	BEAR SNR
FRB 010124	790.3	790	790.238	10.6	7.5	11.25	10.6	22.53	23.0684
FRB 010621	745	748	749.395	7	10	7.5	16.3	15.7427	16.1699
FRB 010724	375	374	930.767	20	24	1529	100	34.4823	50.6785
FRB 090625	899.55	899	899.889	1.92	2.56	1.92	30	23.9272	24.1128
FRB 110220	944.38	946	944.635	6.59	6.4	5.76	54	31.1559	34.5971
FRB 110626	723	724	721.413	1.41	2.56	1.92	12	9.17705	9.43211
FRB 110703	1103.6	1105	1106.37	3.9	3.84	3.2	17	15.0202	14.646
FRB 120127	553.3	554	555.683	1.21	1.28	1.92	13	9.80996	11.2739
FRB 121002	1629.18	1630	1630.05	5.44	6.4	5.76	16	14.4355	15.4915
FRB 130626	952.4	953	953.381	1.98	2.56	1.92	21	14.8354	16.5966
FRB 130628	469.88	471	469.444	0.64	1.28	1.28	29	15.7191	16.5475
FRB 130729	861	854	-	15.61	6.4	-	14	8.30313	-
FRB 140514	561.7	562	-	2.816	3.84	-	16	8.14297	-
FRB 150215	1105.6	1107	1106.37	2.88	2.56	3.2	19	14.2704	14.5193
FRB 121102	557	579	584	3	5.12	5.12	14	22.1387	27.9405
FRB 200428a	337.702	335	-	0.61	1.31072	-	20	10.5442	-
FRB 200428b	337.702	332	-	0.61	1.31072	-	15	10.4817	-
FRB 200428c	337.702	335	-	0.61	1.31072	-	21	8.37221	-

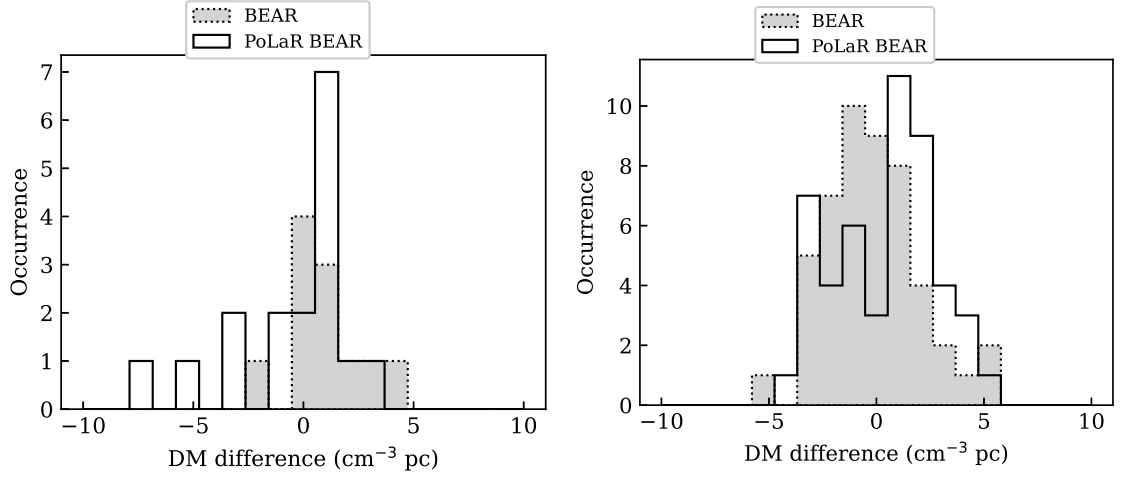


Figure 4.1: Histograms of DM difference in detections from PoLaR BEAR and BEAR for real FRB data (left) and fake FRB data (right).

4.2 Generated FRB data

PoLaR BEAR was able to detect 49 out of 50 FRBs in our sample of fake FRB data. Similarly, the original BEAR was also able to detect 49 out of 50 FRBs. Both programs were not able to detect Fake 19, which has one of the lowest SNR at 9.00864. The detected DM, W, and SNR for PoLaR BEAR and BEAR for each of the fake FRBs are as shown in Table 4.2.

4.3 Difference in detections for PoLaR BEAR and BEAR

4.3.1 Detection DM

Histograms of the DM difference in detections from PoLaR BEAR and BEAR for real FRB data and fake FRB data are shown in Figure 4.1. The outliers here are defined to be data with DM difference of $\pm 10 \text{ cm}^{-3} \text{ pc}$. For real FRB data, PoLaR BEAR has 1 outlier ($22 \text{ cm}^{-3} \text{ pc}$) whereas BEAR has 2 outliers ($555.77 \text{ cm}^{-3} \text{ pc}$, $27 \text{ cm}^{-3} \text{ pc}$). For fake FRB data, both PoLaR BEAR and BEAR exhibited no outliers, with most detections occurring within $\pm 5 \text{ cm}^{-3} \text{ pc}$. In both cases, it can be seen that PoLaR BEAR performs on par with BEAR, with detections close to the true DM.

Table 4.2: Detection results for Fake FRB data using PoLaR BEAR and BEAR.

Fake	True DM ($\text{cm}^{-3} \text{ pc}$)	PoLaR DM ($\text{cm}^{-3} \text{ pc}$)	BEAR ($\text{cm}^{-3} \text{ pc}$)	True W (ms)	PoLaR W (ms)	BEAR W (ms)	True SNR	PoLaR SNR	BEAR SNR
1	566.158	563	565.451	3.47103	3.84	3.2	34.1301	31.3015	32.3983
2	1476.21	1478	1476.53	3.97177	3.84	3.2	46.3679	40.6662	40.4863
3	1858.64	1858	1861.15	2.57209	2.56	3.2	26.5634	23.8261	24.5231
4	399.97	397	396.604	2.77513	2.56	3.2	10.1587	8.70667	8.97403
5	573.649	573	572.429	0.710951	1.28	1.28	16.1083	10.5715	11.0524
6	1187.42	1188	1187.81	3.8433	3.84	3.2	34.5618	29.9834	30.1843
7	1028.33	1027	1028.99	1.66997	2.56	1.92	42.8729	33.8904	38.1275
8	1337.1	1340	1339.68	3.16891	3.84	3.2	45.5356	37.8317	40.721
9	1364.17	1361	1363.64	2.16554	2.56	1.92	15.2655	12.5744	14.0023
10	1321.39	1321	1319.68	4.92548	6.4	5.76	33.4504	29.5878	31.4454
11	1666.28	1667	1665.35	3.77166	3.84	3.2	44.4121	39.6793	40.3442
12	728.46	725	729.275	2.61624	2.56	3.2	20.7568	17.2411	18.0443
13	789.509	786	789.231	1.77699	2.56	1.92	44.6985	34.3899	39.4427
14	1744.95	1742	1744.26	4.58435	3.84	5.76	37.8006	33.5477	35.5756
15	1530.5	1529	1529.48	1.14656	1.28	1.28	47.1532	33.9406	37.9887
16	742.392	744	747.275	3.77817	3.84	3.2	26.9581	23.4275	23.8539
17	1504.54	1508	1509.51	3.39606	3.84	3.2	9.8772	8.65455	9.25259
18	669.927	671	666.341	2.79792	3.84	3.2	11.7874	9.7949	10.5248
19	1287.46	-	-	1.60874	-	-	9.00864	-	-
20	669.849	668	667.341	3.16439	2.56	3.2	23.6871	21.886	22.934
21	1395.44	1397	1396.62	4.48013	3.84	5.76	39.7673	35.3169	35.334
22	678.089	679	679.341	2.73084	2.56	3.2	21.4789	17.189	17.5459
23	393.089	398	396.604	2.40809	2.56	1.92	35.0218	27.1215	29.6006
24	848.94	852	852.165	2.227	2.56	1.92	17.862	16.0703	29.1919
25	846.969	848	846.165	1.62728	1.28	1.92	33.0218	24.5658	26.6359
26	1358.91	1359	1355.66	4.79527	3.84	5.76	18.5694	17.1126	17.8909
27	480.351	482	480.538	2.97478	2.56	3.2	42.4061	36.258	38.868
28	1668.8	1671	1670.35	2.42997	2.56	1.92	29.9655	25.6359	25.8296
29	359.856	364	357.648	4.1512	3.84	3.2	31.7901	25.3873	26.919
30	426.874	428	427.582	1.36033	1.28	1.28	28.9338	21.0301	24.2949
31	1308.65	1311	1312.67	2.71006	3.84	3.2	11.783	10.4659	11.039
32	352.708	354	352.648	0.863634	1.28	1.28	28.142	18.2329	21.6419
33	745.125	747	747.275	0.82552	1.28	1.28	32.431	20.4732	23.1195
34	1355.43	1358	1356.66	2.69499	2.56	3.2	34.6861	28.9677	30.6762
35	741.125	737	741.275	2.97293	3.84	3.2	11.9684	10.4464	11.0272
36	1046.19	1047	1044.97	3.98829	3.84	3.2	18.2477	15.8839	15.2783
37	1199.7	1202	1199.81	1.4724	1.28	1.92	17.7535	13.5037	14.4868
38	518.282	519	517.495	4.72503	3.84	5.76	49.626	40.4404	43.56
39	1799.01	1802	1796.22	4.07805	3.84	3.2	23.5333	22.0723	21.9321
40	670.819	668	665.341	2.36506	2.56	3.2	19.3561	15.944	16.13
41	1688.62	1686	1686.33	0.997483	1.28	1.28	40.5665	25.9701	30.3779
42	1195.6	1197	1195.81	1.85354	2.56	1.92	30.0239	23.9527	25.8458
43	1869.7	1868	1868.15	1.82071	2.56	1.92	24.1694	21.2072	21.7146
44	587.108	591	585.429	3.61604	3.84	3.2	11.8553	11.8643	13.0866
45	601.626	604	598.407	4.16235	3.84	3.2	33.3841	29.8459	29.7412
46	746.818	746	744.275	2.50385	2.56	3.2	9.14934	8.54968	8.387
47	1268.11	1272	1269.75	1.02883	1.28	1.28	15.4958	10.3593	12.6025
48	1818.44	1818	1818.2	4.73783	3.84	5.76	40.2606	34.5793	36.6491
49	1734.89	1734	1733.29	2.3775	2.56	3.2	40.4545	33.3137	33.9313
50	917.338	915	918.099	3.38351	3.84	3.2	40.1697	33.9579	36.37

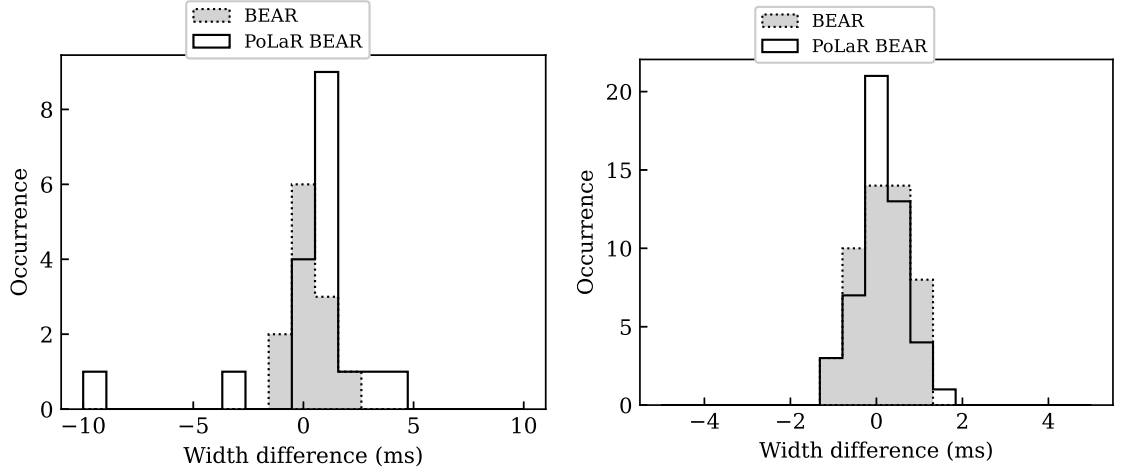


Figure 4.2: Histograms of W difference in detections from PoLaR BEAR and BEAR for real FRB data (left) and fake FRB data (right).

4.3.2 Detection W

Histograms of the W difference in detections from PoLaR BEAR and BEAR for real FRB data and fake FRB data are shown in Figure 4.2. The outliers here are defined to be data with W difference of ± 10 ms. For real FRB data, PoLaR BEAR exhibited no outliers whereas BEAR has 1 outlier (1509 ms). For fake FRB data, both PoLaR BEAR and BEAR exhibited no outliers, with most detections occurring within ± 2 ms. It can be seen that for real FRBs, detections from BEAR do have smaller errors whereas PoLaR BEAR reports larger W . On the other hand, for fake FRBs, PoLaR BEAR was much more consistent with much more detections occurring close to the true W .

4.3.3 Detection SNR

Histograms of the SNR difference in detections from PoLaR BEAR and BEAR for real FRB data and fake FRB data are shown in Figure 4.3. The outliers here are defined to be data with SNR difference of ± 30 . For real FRB data, PoLaR BEAR exhibited no outliers whereas BEAR has 1 outlier (-49.32). For fake FRB data, both PoLaR BEAR and BEAR exhibited no outliers, with most detections occurring within ± 10 . In both cases, PoLaR BEAR performs as well as BEAR.

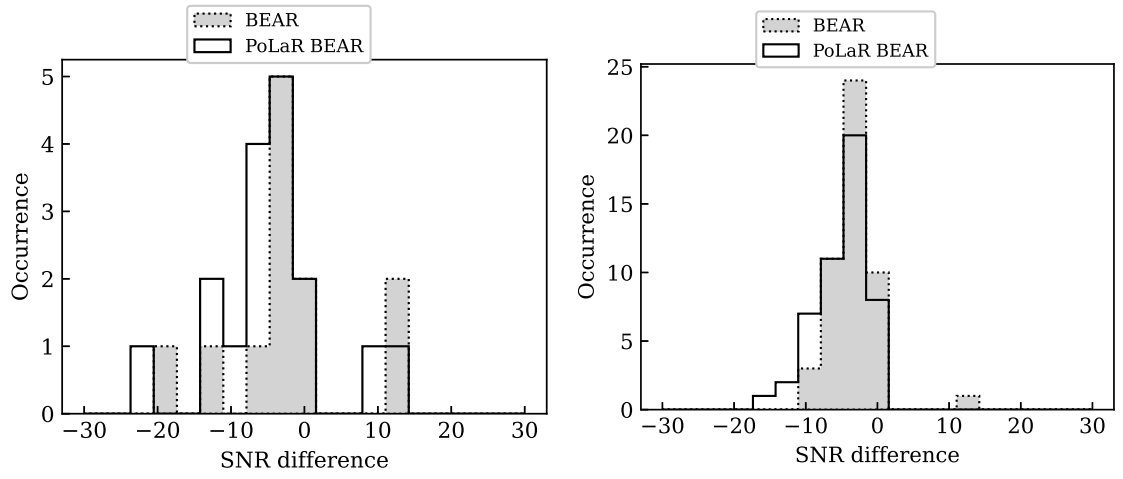


Figure 4.3: Histograms of SNR difference in detections from PoLaR BEAR and BEAR for real FRB data (left) and fake FRB data (right).

CHAPTER 5: DISCUSSIONS

5.1 Performance Quantization

To further quantify the performance of PoLaR BEAR, the average deviations in the detection parameters were observed. Table 5.1 and 5.2 shows the average deviations in the detections for PoLaR BEAR and BEAR for both real FRB data and fake FRB data respectively. For real FRB data, it can be seen that PoLaR BEAR performs significantly better than BEAR for detection DM and W, and only slightly worse for detection SNR. For fake FRB data, it can be seen that PoLaR BEAR performs slightly worse than BEAR for detection DM and SNR, and slightly better for detection W. Therefore, it can be confirmed that PoLaR BEAR performs comparably well with BEAR.

There was also one significant outlier for detections in BEAR that were not present in PoLaR BEAR, namely FRB 010724. BEAR detected a DM of $930.767 \text{ cm}^{-3} \text{ pc}$, which is $555.767 \text{ cm}^{-3} \text{ pc}$ away from the actual value, whereas PoLaR BEAR reported a DM of $374 \text{ cm}^{-3} \text{ pc}$. BEAR also detected a W of 1529 ms, which is 1509 ms away from the actual value, whereas PoLaR BEAR reported a W of 24 ms. Figure 5.1 shows the candidate plot of the detection in PoLaR BEAR. A large decrease in flux after the burst can be seen due to saturation of the receiver, causing the inaccurate detection in BEAR.

Table 5.1: Average deviations in the detection parameters using PoLaR BEAR and BEAR for real FRB data.

Parameter	DM ($\text{cm}^{-3} \text{ pc}$)	W (ms)	SNR
PoLaR BEAR	2.9953	1.6203	10.4972
BEAR	45.9694	116.6431	9.9726

Table 5.2: Average deviations in the detection parameters using PoLaR BEAR and BEAR for fake FRB data.

Parameter	DM ($\text{cm}^{-3} \text{ pc}$)	W (ms)	SNR
PoLaR BEAR	2.0530	0.4282	5.0371
BEAR	1.7404	0.5089	3.8685

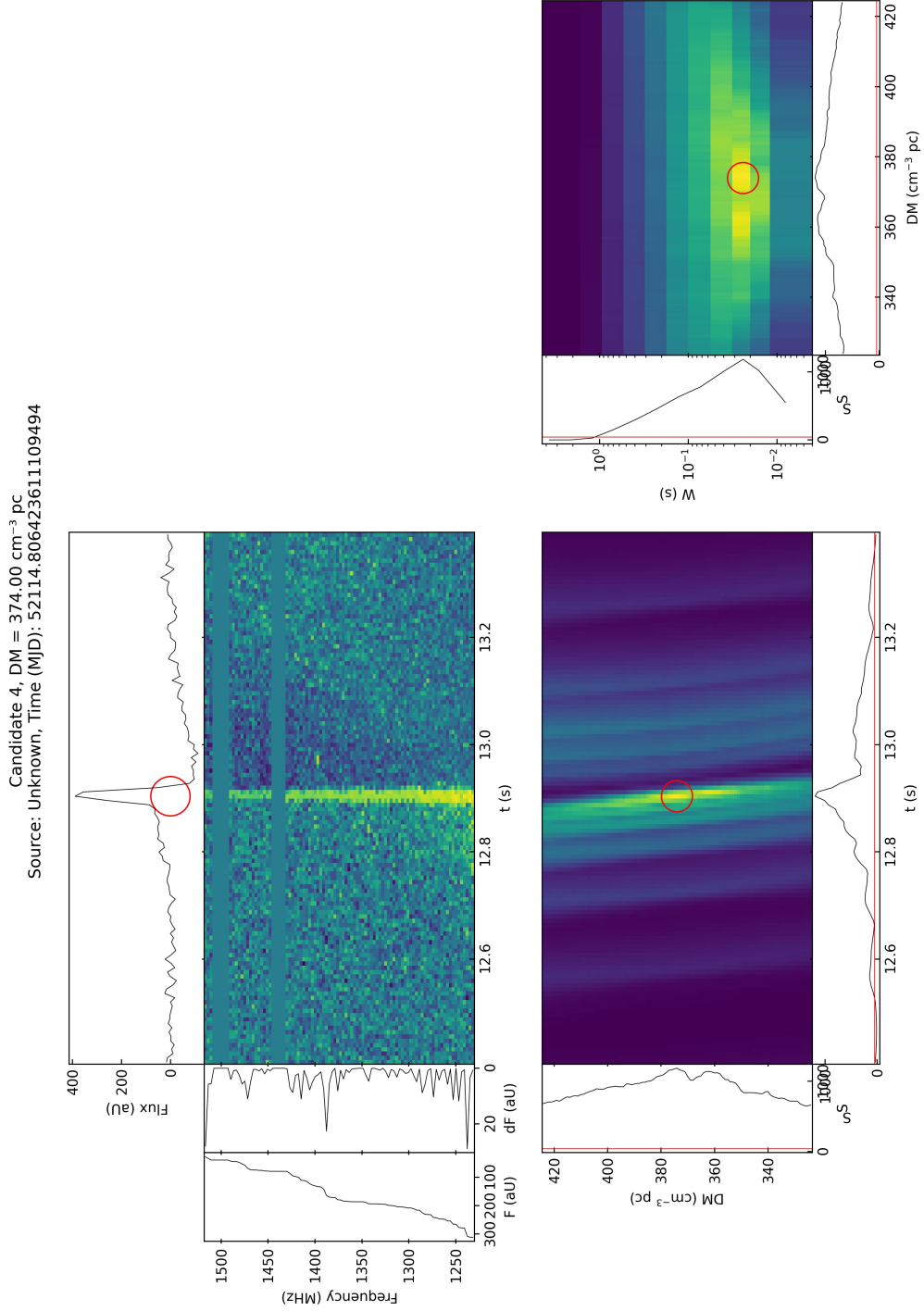


Figure 5.1: PoLaR BEAR candidate output for FRB 010724.

5.2 Underestimation of SNR

In general, the SNRs are detected by PoLaR BEAR and BEAR can be seen to be slightly lower than that of the true values. This is expected as inaccurate DM and W values when performing the calculation for S would result in lower S values, and consequently lower detected SNR. For a DM offset of δDM , the ratio between the SNR detected and the true SNR is (Cordes & McLaughlin, 2003)

$$\frac{\text{SNR}}{\text{SNR}_0} = \frac{\sqrt{\pi}}{2} \zeta^{-1} \text{erf } \zeta \quad (5.1)$$

where SNR_0 is the true SNR if the dedispersion is performed at the true DM. ζ is the ratio between the time delay caused by the DM offset and pulse width given by

$$\zeta = 6.91 \times 10^{-3} \delta\text{DM} \frac{\Delta\nu_{\text{MHz}}}{W_{\text{ms}} \nu_{\text{GHz}}^3} \quad (5.2)$$

As for a W offset of δW , the SNR ratio becomes (Men et al., 2019)

$$\frac{\text{SNR}}{\text{SNR}_0} = \begin{cases} \frac{W}{W+\delta W}, & \text{for } \delta W \geq 0, \\ \frac{W+\delta W}{W}, & \text{for } \delta W < 0 \end{cases} \quad (5.3)$$

For any non-zero offset in DM and W, both cases result in a lower detection SNR compared to SNR_0 , shown in Figure 5.2.

5.3 Differences between PoLaR BEAR and BEAR

Other than the differences between Python and C++, there are two main differences between PoLaR BEAR and BEAR. The first is the division of trial DMs. In BEAR, subband dedispersion is used to improve its efficacy (Barsdell et al., 2012). Subband dedispersion is an approximation approach in reducing the computation cost of dedispersion. The process

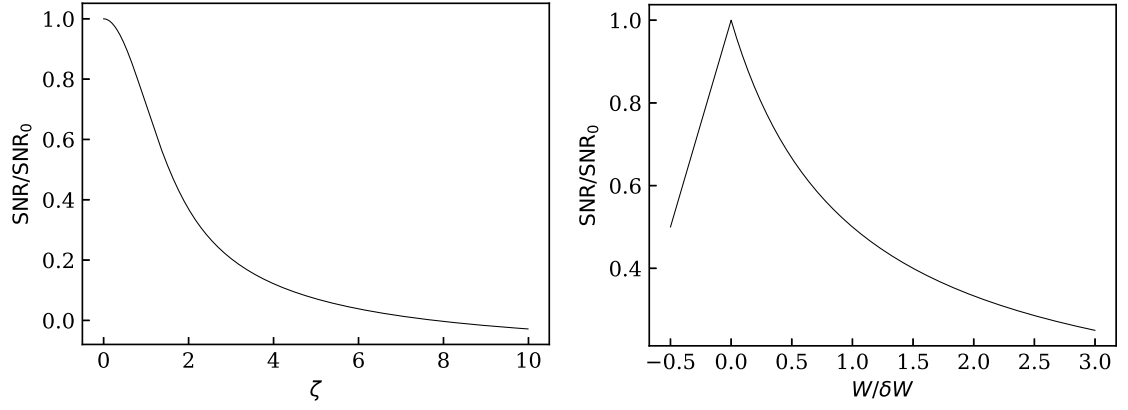


Figure 5.2: Graph of SNR deviation due to DM offset i.e. $\zeta \propto \delta\text{DM}$ (left), and due to W offset i.e. $\delta W/W$ (right). Detected SNR decreases for any non-zero δDM and $\delta W/W$.

involves splitting up the DM range into several subranges, each centered around a nominal DM value. The frequency channels are also partitioned into subbands. The delays for every nominal DMs are subtracted from the subbands, resulting in partially dedispersed subbands. The data is then passed through the usual dedispersion at the remaining DMs. This results in a trial DM array with differing increments depending on the nominal DM, usually larger increments at higher DMs, as shown in Table 5.3 (Magro et al., 2011).

Table 5.3: Example of a subband dedispersion plan for a pulsar survey. $\Delta\text{Sub}_{\text{DM}}$ refers to the DM step between two successive nominal DM values, ΔDM is the finer step used for creating the dedispersed time series around a particular nominal DM value.

Pass	Low DM ($\text{cm}^{-3} \text{ pc}$)	High DM ($\text{cm}^{-3} \text{ pc}$)	ΔDM ($\text{cm}^{-3} \text{ pc}$)	$\Delta\text{Sub}_{\text{DM}}$ ($\text{cm}^{-3} \text{ pc}$)
1	0.00	53.46	0.03	0.66
2	53.46	88.26	0.05	1.2
3	88.26	150.66	0.10	2.4

However, in PoLaR BEAR, I opted to set the DM range and a single increment in the beginning (usually from 1 to 2000 $\text{cm}^{-3} \text{ pc}$ with increments of 1 $\text{cm}^{-3} \text{ pc}$) and use the usual brute force dedispersion. This is because the program is aimed to allow for an easier understanding in FRB detection instead of performance.

Another difference is in the definition of the detection time or also known as the pulse

epoch, t_0 . In BEAR, t_0 is defined to be the beginning of the pulse, allowing it to utilize efficient looping methods for the calculation of S . However in PoLaR BEAR, t_0 is defined to be in the middle of the pulse, allowing the usage of convolution in the program which follows the usual Python style.

5.4 GPU Dedispersion

As stated in Magro et al., 2011, graphics processing unit or GPU computation can also speed up dedispersion to improve real time detection of radio transients. Using NVIDIA's CUDA cores, dedispersion can be parallelized over many GPU threads, simultaneously operating on many different DMs. Tests have shown that GPUs speed up dedispersion by 50 to 200 times (Magro et al., 2011) or at least by 9 times (Barsdell et al., 2012) when compared to single-threaded CPU implementation. This is applied in many FRB searches e.g. AMBER used on the Westerbork Telescope (Sclocco et al., 2020) and the Medicina BEST-2 transient search pipeline (Magro, Hickish, & Adami, 2013).

In Python, two packages allows python to utilize GPU to speed up numpy functions, namely CuPy and Numba. In this case, CuPy was used as it is a more complete reimplementation of Numpy using the GPU, compared to Numba where custom algorithms tailored to its format is required (Okuta, Unno, Nishino, Hido, & Crissman, 2017).

To test the performance increase of GPU dedispersion in this case, the data was generated using the same method with the same properties as for fake FRB, with varying observation times i.e. 0.125, 0.25, 0.5, 1, 2, and 5 minutes, and varying number of frequency channels i.e. 128, 256, 512, and 1024 frequency channels. The data is also downsampled by 20 to reduce computation time. The data is then dedispersed using both brute force dedispersion with `numpy.roll` and a modified dedispersion with `cupy.roll` at a single DM ($1000 \text{ cm}^{-3} \text{ pc}$), as dedispersion at different DMs should not affect the performance significantly. Note that the GPU used here is the GTX 1660 Ti, with 1536

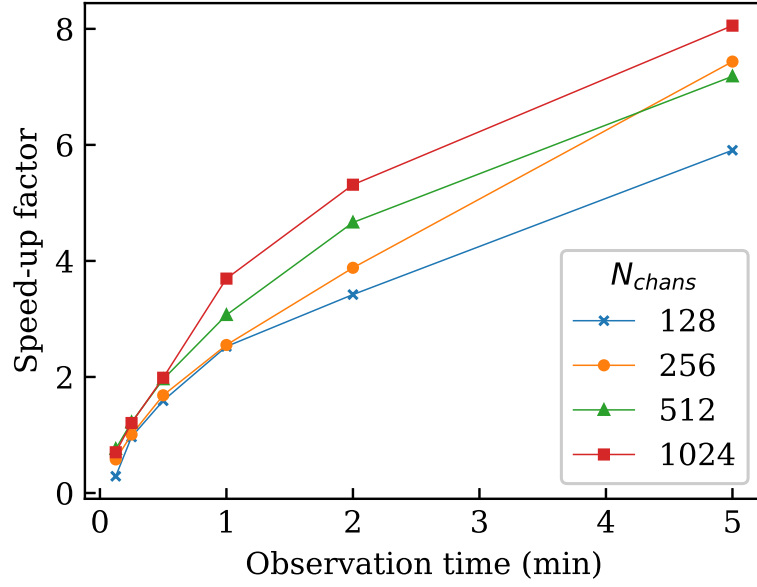


Figure 5.3: Graph of speed-up factor between GPU dedispersion and usual CPU dedispersion for different data lengths and different number of frequency channels.

CUDA cores rated at a maximum of 169.9 GFLOPS, and 6 GB of memory.

Figure 5.3 shows the graph of the speed-up factor of GPU dedispersion compared to the brute force CPU implementation for different data length/observation time, as well as at different number of frequency channels. The speed-up factor can be seen to increase with observation times up to a factor of 8, but shorter observation times result in speed-up factors of less than one i.e. GPU dedispersion slower than CPU implementation, which could be due to the memory transfer latency between the RAM and the GPU memory. Therefore, implementation of GPU dedispersion in PoLaR BEAR using CuPy can be beneficial to improve its performance. Note that the benefits may scale further at larger observation time, but requires a much larger amount of GPU memory, which is the reason that the tests was only done for data up to 5 minutes observation time with 1024 frequency channels.

CHAPTER 6: SUMMARY

FRBs are bright, broadband radio emission ranging from milliseconds or less. The key characteristic of FRBs is their dispersion measure or DM, seen as a frequency-dependent delay in the signal. Most FRBs have DMs more than the contribution from our galaxy, suggesting its extragalactic nature. The signal characteristics seem to suggest that FRBs come from magnetars. FRBs are usually detected using single-dish telescopes, and the data is passed through pipelines that perform the detection and analysis of the FRBs.

The first objective of this project was to understand FRB detection methods, which are mainly done using matched filtering and the likelihood statistic ratio.

The second objective was to develop a program that independently searches for FRBs in radio telescope data. Here, I created the PoLaR BEAR independent FRB detection program that searches for FRBs in radio telescope data in Python, based on BEAR. The program involves many functions, where the three main ones are RFI mitigation, dedispersion, and matched filtering. RFI mitigation is performed by zapping frequency channels with RFI, and by using ZDMF to remove any narrow-band short-duration RFI with no dispersive nature. Dedispersion shifts the data to compensate for the dispersion to maximize the SNR of the FRB. Matched filtering then calculates the SNR in the data based on the likelihood statistic ratio for all DM, time, and W, then peaks in the SNR denotes an FRB detection.

The third objective was to compare the performance of the program developed with BEAR. PoLaR BEAR was tested with real FRB data and fake FRB data generated using Python. PoLaR BEAR performs well with small deviations in the detection parameters compared to the actual parameters, comparable to that of BEAR. The detection SNR are also slightly underestimated as expected due to deviations in DM and W.

The final objective was to test the performance increase for GPU dedispersion. In this case, GPU dedispersion was implemented in PoLar BEAR using CuPy, and dedispersion can be sped up by up to 8 times compared to brute force CPU dedispersion.

With this, an independent FRB detection pipeline was successfully created using Python. Detecting more FRBs will help in pinpointing the correct origin of FRBs. If they are from magnetars, FRBs would be a crucial way to study their properties e.g. the origin of their strong magnetic fields, their composition, their formation origin, and the types of stars that would transition into them.

REFERENCES

- Bannister, K. W., Shannon, R. M., Macquart, J.-P., Flynn, C., Edwards, P. G., O'Neill, M., . . . Westmeier, T. (2017, May). The detection of an extremely bright fast radio burst in a phased array feed survey. *The Astrophysical Journal*, 841(1), L12. doi: 10.3847/2041-8213/aa71ff
- Barsdell, B. R., Bailes, M., Barnes, D. G., Fluke, C. J. (2012, March). Accelerating incoherent dedispersion. *Monthly Notices of the Royal Astronomical Society*, 422(1), 379–392. doi: 10.1111/j.1365-2966.2012.20622.x
- Bochenek, C. D., Ravi, V., Dong, D. (2021, January). Localized fast radio bursts are consistent with magnetar progenitors formed in core-collapse supernovae. *The Astrophysical Journal*, 907(2), L31. doi: 10.3847/2041-8213/abd634
- Caleb, M., Flynn, C., Bailes, M., Barr, E. D., Bateman, T., Bhandari, S., . . . Krishnan, V. V. (2016, March). Fast radio transient searches with UTMOST at 843 MHz. *Monthly Notices of the Royal Astronomical Society*, 458(1), 718–725. doi: 10.1093/mnras/stw109
- CHIME/FRB Collaboration, Amiri, M., Bandura, K., Berger, P., Bhardwaj, M., Boyce, M. M., . . . Wiebe, D. V. (2018, August). The CHIME fast radio burst project: System overview. *The Astrophysical Journal*, 863(1), 48. doi: 10.3847/1538-4357/aad188
- CHIME/FRB Collaboration, Andersen, B. C., Bandura, K. M., Bhardwaj, M., Bij, A., Boyce, M. M., . . . Zwaniga, A. V. (2020, November). A bright millisecond-duration radio burst from a galactic magnetar. *Nature*, 587(7832), 54–58. doi: 10.1038/s41586-020-2863-y
- Cordes, J. M., McLaughlin, M. A. (2003, October). Searches for fast radio transients. *The Astrophysical Journal*, 596(2), 1142–1154. doi: 10.1086/378231
- Cruces, M., Spitler, L. G., Scholz, P., Lynch, R., Seymour, A., Hessels, J. W. T., . . . Munjal, S. (2020, October). Repeating behaviour of FRB 121102: periodicity, waiting times, and energy distribution. *Monthly Notices of the Royal Astronomical Society*, 500(1), 448–463. doi: 10.1093/mnras/staa3223
- Dai, J.-P., Xia, J.-Q. (2021, March). Reconstruction of baryon fraction in intergalactic medium through dispersion measurements of fast radio bursts. *Monthly Notices of*

- Dai, Z. G., Wang, J. S., Wu, X. F., Huang, Y. F. (2016, September). Repeating fast radio bursts from highly magnetized pulsars traveling through asteroid belts. *The Astrophysical Journal*, 829(1), 27. doi: 10.3847/0004-637x/829/1/27
- Fisz, M. (1963). *Probability theory and mathematical statistics*. New York: Wiley. (ISBN: 9780471262503)
- Hagstotz, S., Reischke, R., Lilow, R. (2021). *A new measurement of the hubble constant using fast radio bursts*. Retrieved from <https://arxiv.org/abs/2104.04538>
- James, C. W., Bannister, K. W., Macquart, J.-P., Ekers, R. D., Osłowski, S., Shannon, R. M., . . . Whiting, M. T. (2019). The performance and calibration of the CRAFT fly’s eye fast radio burst survey. *Publications of the Astronomical Society of Australia*, 36. doi: 10.1017/pasa.2019.1
- Katz, J. I. (2020, October). The FRB–SGR connection. *Monthly Notices of the Royal Astronomical Society*, 499(2), 2319–2326. doi: 10.1093/mnras/staa3042
- Keane, E. F., Johnston, S., Bhandari, S., Barr, E., Bhat, N. D. R., Burgay, M., . . . Bassa, C. (2016, February). The host galaxy of a fast radio burst. *Nature*, 530(7591), 453–456. doi: 10.1038/nature17140
- Keane, E. F., SUPERB Collaboration. (2017, November). Fast radio bursts: Searches, sensitivities & implications. In *The fourteenth marcel grossmann meeting*. WORLD SCIENTIFIC. doi: 10.1142/9789813226609_0360
- Keith, M. J., Jameson, A., Straten, W. V., Bailes, M., Johnston, S., Kramer, M., . . . Stappers, B. W. (2010, September). The High Time Resolution Universe Pulsar Survey - I. System configuration and initial discoveries. *Monthly Notices of the Royal Astronomical Society*, 409(2), 619–627. doi: 10.1111/j.1365-2966.2010.17325.x
- Kocz, J., Briggs, F. H., Reynolds, J. (2010, November). Radio frequency interference removal through the application of spatial filtering techniques on the Parkes Multibeam Receiver. *The Astronomical Journal*, 140(6), 2086–2094. doi: 10.1088/0004-6256/140/6/2086

- Lorimer, D. (2007, February). *Sigproc-v4.0: Pulsar signal processing programs*. West Virginia University. Retrieved from https://casper.berkeley.edu/svn/trunk/projects/dig_int_kurt_spec/sigproc-4.3/sigproc.pdf
- Lorimer, D. R., Bailes, M., McLaughlin, M. A., Narkevic, D. J., Crawford, F. (2007, November). A bright millisecond radio burst of extragalactic origin. *Science*, 318(5851), 777–780. doi: 10.1126/science.1147532
- Luo, R., Wang, B. J., Men, Y. P., Zhang, C. F., Jiang, J. C., Xu, H., . . . Zhu, Y. (2020, October). Diverse polarization angle swings from a repeating fast radio burst source. *Nature*, 586(7831), 693–696. doi: 10.1038/s41586-020-2827-2
- Lyubarsky, Y. (2014, April). A model for fast extragalactic radio bursts. *Monthly Notices of the Royal Astronomical Society: Letters*, 442(1), L9–L13. doi: 10.1093/mnrasl/slu046
- Macquart, J.-P., Prochaska, J. X., McQuinn, M., Bannister, K. W., Bhandari, S., Day, C. K., . . . Tejos, N. (2020, May). A census of baryons in the Universe from localized fast radio bursts. *Nature*, 581(7809), 391–395. doi: 10.1038/s41586-020-2300-2
- Madison, D. R., Agarwal, D., Aggarwal, K., Young, O., Cromartie, H. T., Lam, M. T., . . . Wharton, R. S. (2019, December). A deep targeted search for fast radio bursts from the sites of low-redshift short gamma-ray bursts. *The Astrophysical Journal*, 887(2), 252. doi: 10.3847/1538-4357/ab58c3
- Magro, A., Hickish, J., Adami, K. Z. (2013, September). Multibeam GPU transient pipeline for the Medicina BEST-2 array. *Journal of Astronomical Instrumentation*, 02(01), 1350008. doi: 10.1142/s2251171713500086
- Magro, A., Karastergiou, A., Salvini, S., Mort, B., Dulwich, F., Adami, K. Z. (2011, September). Real-time, fast radio transient searches with GPU de-dispersion. *Monthly Notices of the Royal Astronomical Society*, 417(4), 2642–2650. doi: 10.1111/j.1365-2966.2011.19426.x
- Marcote, B., Nimmo, K., Hessels, J. W. T., Tendulkar, S. P., Bassa, C. G., Paragi, Z., . . . Zwaniga, A. V. (2020, January). A repeating fast radio burst source localized to a nearby spiral galaxy. *Nature*, 577(7789), 190–194. doi: 10.1038/s41586-019-1866-z
- Masui, K., Lin, H.-H., Sievers, J., Anderson, C. J., Chang, T.-C., Chen, X., . . . Yadav,

- J. K. (2015, December). Dense magnetized plasma associated with a fast radio burst. *Nature*, 528(7583), 523–525. doi: 10.1038/nature15769
- Men, Y. P., Luo, R., Chen, M. Z., Hao, L. F., Lee, K. J., Li, J., . . . Zhang, C. F. (2019, July). Piggyback search for fast radio bursts using Nanshan 26 m and Kunming 40 m radio telescopes – I. Observing and data analysis systems, discovery of a mysterious peryton. *Monthly Notices of the Royal Astronomical Society*, 488(3), 3957–3971. doi: 10.1093/mnras/stz1931
- Metzger, B. D., Fang, K., Margalit, B. (2020, October). Neutrino counterparts of fast radio bursts. *The Astrophysical Journal*, 902(1), L22. doi: 10.3847/2041-8213/abbb88
- Metzger, B. D., Margalit, B., Sironi, L. (2019, March). Fast radio bursts as synchrotron maser emission from decelerating relativistic blast waves. *Monthly Notices of the Royal Astronomical Society*, 485(3), 4091–4106. doi: 10.1093/mnras/stz700
- Michilli, D., Masui, K. W., Mckinven, R., Cubranic, D., Bruneault, M., Brar, C., . . . Vanderlinde, K. (2021, April). An analysis pipeline for CHIME/FRB full-array baseband data. *The Astrophysical Journal*, 910(2), 147. doi: 10.3847/1538-4357/abe626
- Murase, K., Kashiyama, K., Mészáros, P. (2016, June). A burst in a wind bubble and the impact on baryonic ejecta: high-energy gamma-ray flashes and afterglows from fast radio bursts and pulsar-driven supernova remnants. *Monthly Notices of the Royal Astronomical Society*, 461(2), 1498–1511. doi: 10.1093/mnras/stw1328
- Ocker, S. K., Cordes, J. M., Chatterjee, S. (2021, April). Constraining galaxy halos from the dispersion and scattering of fast radio bursts and pulsars. *The Astrophysical Journal*, 911(2), 102. doi: 10.3847/1538-4357/abeb6e
- Okuta, R., Unno, Y., Nishino, D., Hido, S., Crissman. (2017). Cupy : A NumPy-compatible library for NVIDIA GPU calculations.. Retrieved from http://learningsys.org/nips17/assets/papers/paper_16.pdf
- Pagano, M., Fronenberg, H. (2021, May). Constraining the epoch of reionization with highly dispersed fast radio bursts. *Monthly Notices of the Royal Astronomical Society*, 505(2), 2195–2206. doi: 10.1093/mnras/stab1438
- Pang, D., Goseva-Popstojanova, K., Devine, T., McLaughlin, M. (2018, August). A novel single-pulse search approach to detection of dispersed radio pulses using clustering

and supervised machine learning. *Monthly Notices of the Royal Astronomical Society*, 480(3), 3302–3323. doi: 10.1093/mnras/sty1992

Patel, C., Agarwal, D., Bhardwaj, M., Boyce, M. M., Brazier, A., Chatterjee, S., ... van Leeuwen, J. (2018, December). PALFA single-pulse pipeline: New pulsars, rotating radio transients, and a candidate fast radio burst. *The Astrophysical Journal*, 869(2), 181. doi: 10.3847/1538-4357/aace65

Petroff, E., Hessels, J. W. T., Lorimer, D. R. (2019, May). Fast radio bursts. *The Astronomy and Astrophysics Review*, 27(1). doi: 10.1007/s00159-019-0116-6

Rane, A., Lorimer, D. R., Bates, S. D., McMann, N., McLaughlin, M. A., Rajwade, K. (2015, November). A search for rotating radio transients and fast radio bursts in the Parkes high-latitude pulsar survey. *Monthly Notices of the Royal Astronomical Society*, 455(2), 2207–2215. doi: 10.1093/mnras/stv2404

Ransom, S. (n.d.). *Searching for pulsars with PRESTO*. NRAO/UVa. Retrieved from https://www.cv.nrao.edu/~sransom/PRESTO_search_tutorial.pdf

Ravi, V., Shannon, R. M., Bailes, M., Bannister, K., Bhandari, S., Bhat, N. D. R., ... Vedantham, H. K. (2016, November). The magnetic field and turbulence of the cosmic web measured using a brilliant fast radio burst. *Science*, 354(6317), 1249–1252. doi: 10.1126/science.aaf6807

Reischke, R., Hagstotz, S., Lilow, R. (2021). *Consistent equivalence principle tests with fast radio bursts*. Retrieved from <https://arxiv.org/abs/2102.11554>

Sanidas, S., Caleb, M., Driessen, L., Morello, V., Rajwade, K., Stappers, B. W. (2017, September). MeerTRAP: A pulsar and fast transients survey with MeerKAT. *Proceedings of the International Astronomical Union*, 13(S337), 406–407. doi: 10.1017/s1743921317009310

Sclocco, A., Heldens, S., van Werkhoven, B. (2020, July). AMBER: A real-time pipeline for the detection of single pulse astronomical transients. *SoftwareX*, 12, 100549. doi: 10.1016/j.softx.2020.100549

Shannon, R. M., Macquart, J.-P., Bannister, K. W., Ekers, R. D., James, C. W., Osłowski, S., ... Riseley, C. J. (2018, October). The dispersion–brightness relation for fast radio bursts from a wide-field survey. *Nature*, 562(7727), 386–390. doi: 10.1038/s41586-018-0588-y

- Spitler, L. G., Cordes, J. M., Hessels, J. W. T., Lorimer, D. R., McLaughlin, M. A., Chatterjee, S., . . . Fehrmann, H. (2014, July). Fast radio burst discovered in the Arecibo Pulsar ALFA Survey. *The Astrophysical Journal*, 790(2), 101. doi: 10.1088/0004-637x/790/2/101
- Totani, T. (2013, October). Cosmological fast radio bursts from binary neutron star mergers. *Publications of the Astronomical Society of Japan*, 65(5), L12. doi: 10.1093/pasj/65.5.112
- Vaĭnshteĭn, L., Zubakov, V. (1970). *Extraction of signals from noise*. Dover Publications. (ISBN: 9780486626253)
- Wang, H., Miao, X., Shao, L. (2021). *Bounding the photon mass with cosmological propagation of fast radio bursts*. Retrieved from <https://arxiv.org/abs/2103.15299>
- Wang, W.-Y., Zhang, B., Chen, X., Xu, R. (2020, September). On the magnetoionic environments of fast radio bursts. *Monthly Notices of the Royal Astronomical Society*, 499(1), 355–361. doi: 10.1093/mnras/staa2693
- Wei, J.-J., Gao, H., Wu, X.-F., Mészáros, P. (2015, December). Testing Einstein’s equivalence principle with fast radio bursts. *Physical Review Letters*, 115(26). doi: 10.1103/physrevlett.115.261101
- Wu, X.-F., Zhang, S.-B., Gao, H., Wei, J.-J., Zou, Y.-C., Lei, W.-H., . . . Mészáros, P. (2016, April). Constraints on the photon mass with fast radio bursts. *The Astrophysical Journal*, 822(1), L15. doi: 10.3847/2041-8205/822/1/L15
- Zhang, B. (2016, August). Mergers of charged black holes: Gravitational-wave events, short gamma-ray bursts, and fast radio bursts. *The Astrophysical Journal*, 827(2), L31. doi: 10.3847/2041-8205/827/2/L31
- Zhang, C. F., Xu, J. W., Men, Y. P., Deng, X. H., Xu, H., Jiang, J. C., . . . Ma, Z. Y. (2021, March). Fast radio burst detection in the presence of coloured noise. *Monthly Notices of the Royal Astronomical Society*, 503(4), 5223–5231. doi: 10.1093/mnras/stab823
- Zhou, B., Li, X., Wang, T., Fan, Y.-Z., Wei, D.-M. (2014, May). Fast radio bursts as a cosmic probe? *Physical Review D*, 89(10). doi: 10.1103/physrevd.89.107303